


Mutation order in acute myeloid leukemia identifies uncommon patterns of evolution and illuminates phenotypic heterogeneity

Working Paper**Author(s):**

Schwede, Matthew; Jahn, Katharina; Kuipers, Jack; Miles, Linde A.; Bowman, Robert L.; Robinson, Troy; Furudate, Ken; Uryu, Hidetaka; Tanaka, Tomoyuki; Sasaki, Yuya; Ediriwickrema, Asiri; Benard, Brooks; Gentles, Andrew J.; Levine, Ross; [Beerenwinkel, Niko](#) ; Takahashi, Koichi; Majeti, Ravindra

Publication date:

2023-11-06

Permanent link:

<https://doi.org/10.3929/ethz-b-000653062>

Rights / license:

[Creative Commons Attribution 4.0 International](#)

Originally published in:

Research Square, <https://doi.org/10.21203/rs.3.rs-3516536/v1>

Mutation order in acute myeloid leukemia identifies uncommon patterns of evolution and illuminates phenotypic heterogeneity

Matthew Schwede^{*1,2}, Katharina Jahn^{*3,4,5}, Jack Kuipers^{4,5}, Linde A. Miles^{6,7}, Robert L. Bowman⁸, Troy Robinson^{9,10}, Ken Furudate¹¹, Hidetaka Uryu¹¹, Tomoyuki Tanaka¹¹, Yuya Sasaki¹¹, Asiri Ediriwickrema^{1,12,13}, Brooks Benard¹⁴, Andrew J. Gentles^{2,14,15}, Ross Levine^{9,16,17}, Niko Beerenwinkel^{+4,5}, Koichi Takahashi⁺¹¹, Ravindra Majeti^{+1,12,13}

1. Department of Medicine, Division of Hematology, Stanford University, Stanford, CA, USA
2. Department of Biomedical Data Science, Stanford University, School of Medicine, Stanford, California, USA
3. Biomedical Data Science, Institute for Computer Science, Free University of Berlin, Berlin, Germany
4. Department of Biosystems Science and Engineering, ETH Zurich, Basel, Switzerland
5. SIB Swiss Institute of Bioinformatics, Lausanne, Switzerland
6. Division of Experimental Hematology, Cincinnati Children's Hospital Medical Center, Cincinnati, OH, USA
7. Department of Pediatrics, University of Cincinnati, Cincinnati OH USA
8. Department of Cancer Biology, Perelman School of Medicine, University of Pennsylvania, Philadelphia, PA, USA
9. Human Oncology and Pathogenesis Program, Molecular Cancer Medicine Service, Memorial Sloan Kettering Cancer Center, New York, New York, USA
10. Louis V. Gerstner Jr. Graduate School of Biomedical Sciences, Memorial Sloan Kettering Cancer Center, New York, New York, USA
11. Department of Leukemia, The University of Texas MD Anderson Cancer Center, Houston, TX.
12. Cancer Institute, Stanford University School of Medicine, Stanford, CA.
13. Institute for Stem Cell Biology and Regenerative Medicine, Stanford University School of Medicine, Stanford, CA.
14. Department of Pathology, Stanford University, Stanford, CA, USA
15. Department of Medicine, Stanford Center for Biomedical Informatics Research, Stanford University, Stanford, CA, USA
16. Center for Hematologic Malignancies, Memorial Sloan Kettering Cancer Center, New York, New York, USA
17. Leukemia Service, Department of Medicine, Memorial Sloan Kettering Cancer Center, New York, New York, USA

*These authors contributed equally

43 † Corresponding authors:

44

45 Ravindra Majeti

46 rmajeti@stanford.edu

47

48 Koichi Takahashi

49 KTakahashi@mdanderson.org

50

51 Niko Beerenwinkel

52 niko.beerenwinkel@bsse.ethz.ch

53

54

55 Abstract

56 Acute myeloid leukemia (AML) has a poor prognosis and a heterogeneous mutation landscape.
57 Although common mutations are well-studied, little research has characterized how the sequence
58 of mutations relates to clinical features. Using published, single-cell DNA sequencing data from
59 three institutions, we compared clonal evolution patterns in AML to patient characteristics, disease
60 phenotype, and outcomes. Mutation trees, which represent the order of select mutations, were
61 created for 207 patients from targeted panel sequencing data using 1 639 162 cells, 823 mutations,
62 and 275 samples. In 224 distinct orderings of mutated genes, mutations related to DNA
63 methylation typically preceded those related to cell signaling, but signaling-first cases did occur,
64 and had higher peripheral cell counts, increased signaling mutation homozygosity, and younger
65 patient age. Serial sample analysis suggested that *NPM1* and DNA methylation mutations provide
66 an advantage to signaling mutations in AML. Interestingly, *WT1* mutation evolution shared
67 features with signaling mutations, such as *WT1*-early being proliferative and occurring in younger
68 individuals, trends that remained in multivariable regression. Some mutation orderings had a worse
69 prognosis, but this was mediated by unfavorable mutations, not mutation order. These findings
70 add a dimension to the mutation landscape of AML, identifying uncommon patterns of
71 leukemogenesis and shedding light on heterogenous phenotypes.

72

73 Introduction

74 Acute myeloid leukemia (AML) has a dismal prognosis, with a five-year overall survival
75 of approximately 30% (1). The poor outcomes are in part due to AML being a heterogeneous
76 disease, with substantial variability between cases and in the subclones of an individual case (2–
77 4). Recent studies have elucidated the clinical consequences of individual mutations in AML (4)
78 and their interactions (5), but little research has evaluated whether modes of leukemogenesis like
79 mutation order, rather than presence of mutations, are associated with clinical features and
80 outcomes (6,7). Preleukemic cells often harbor mutations related to epigenetic modification, which
81 usually occur before those related to cell signaling (8,9), but whether mutations can also occur in
82 atypical orders, such as signaling mutations first, and the relationship between mutation order and
83 phenotype in AML are poorly characterized.

84 In a related group of disorders, myeloproliferative neoplasms (MPNs), variable mutation
85 order is relevant to disease phenotype and provides insight into pathogenesis. The order of
86 mutations in *TET2* and *JAK2* is associated with *JAK2* homozygosity, patient age, and cell
87 proliferation (6). The composition of hematopoietic stem and progenitor cells (HSPCs) also
88 differs, with single-mutant cells dominating HSPCs in *TET2*-first cases but not in *JAK2*-first cases,
89 suggesting that *TET2* mutations offer a fitness advantage in HSPCs compared to *JAK2* mutations
90 (6).

91 Here, we analyzed AML samples for similar patterns related to mutation order by
92 aggregating large single-cell DNA sequencing (scDNAseq) datasets and using computational tools
93 to create evolutionary trees. We characterize the co-occurrence and order of select mutations and
94 the relationship between mutation order and several clinical features.

95

96 Materials and Methods

97 Data

98 Previously published scDNAseq data of patients with AML came from the MD Anderson
99 Cancer Center (123 patients, 154 samples) (10), Stanford University (14 patients, 38 samples)
100 (11), and Memorial Sloan Kettering (MSK) Cancer Center (91 patients, 116 samples) (12)
101 (Supplementary Figure 1). Three more Stanford patients were included because this analysis
102 included secondary AML, and each contributed three samples (diagnosis, remission, relapse).
103 The sequencing has been described in detail in each respective study. Briefly, data were

104 generated using Mission Bio's Tapestri platform, and FASTQ files had been processed using
105 Mission Bio's Tapestri Pipeline v1. Zygosity was determined using the GATK HaplotypeCaller
106 (13) and did not distinguish homozygosity from loss of heterozygosity.

107 All samples from MSK were processed using a custom targeted 31-gene sequencing
108 panel, and 64 samples from MD Anderson were processed using a custom 37-gene panel. All
109 other samples underwent sequencing using a 19-gene AML-specific panel created by Mission
110 Bio (Supplementary Table 1). All panels included those 19 genes, and for the initial descriptive
111 analyses, all data and mutations were considered.

112 Identifying driver mutations

113 Variants were included if both 1% of cells were mutated (11), and the lower bound of a
114 confidence interval for the number of cells containing the mutation was greater than 10 (12).
115 Variants were considered driver mutations using prior criteria (14,15) (Supplementary Methods),
116 or if they had experimental evidence supporting their pathogenicity (Supplementary Figure 2).
117 Variants were excluded if they are not associated with AML but either appeared in most patients
118 in a dataset or were repeatedly mutated in a low percentage of cells (Supplementary Methods,
119 Supplementary Figure 3).

120 Modeling mutation acquisition

121 Single Cell Inference of Tumor Evolution (SCITE) (16,17) was used to create a mutation
122 tree for each patient. Mutation events were assumed to occur at most once and not to revert to
123 wildtype during a patient's course (infinite sites assumption). We assumed that zygosity has
124 minimal impact on mutation calling and on mutation order inference, so zygosity was ignored
125 when creating trees. When multiple samples were available for a patient, samples were merged
126 into a single mutation matrix where mutations absent at one timepoint but not another were
127 assumed wildtype. When variants of unknown significance were available, they were included in
128 the mutation matrix to inform tree architecture but not for downstream mutation order inference.
129 See Supplementary Methods for additional modeling details.

130

131 Modeling FLT3-ITD variants

132 Several samples had multiple distinct insertion sequences in *FLT3* exons 14 or 15, where
133 *FLT3* internal tandem duplication (FLT3-ITD) mutations occur. However, we suspected that
134 different ITDs in the same patient often represented the same ITD event for the purposes of

135 evolutionary analyses. This is because seemingly distinct ITDs insertions usually shared similar
136 DNA sequences, and different datasets had substantially different numbers of ITDs per patient,
137 suggesting batch effects (Supplementary Figure 4). Thus, we merged ITDs from a patient if
138 insertions started at the same locus and were subsequences of another insertion, if they were all
139 terminal events from the same parent event in a tree, or if not merging ITDs resulted in more
140 poorly supported connections in the tree (“Tree Analysis” below, Supplementary Methods,
141 Supplementary Figure 4).

142

143 Tree analysis

144 Driver mutations, which were summarized as either the genes or biological pathways
145 affected (Supplementary Table 2), were analyzed as trees with R v4.3.0 using the igraph package
146 (18). When merging graphs, the size of an edge or vertex reflected the number of times the same
147 sequence of events starting from the root node was observed in the entire dataset. A mutation
148 was considered “early” if no single-cell mutations preceded it (Supplementary Methods). The
149 binomial test and exact multinomial test (19) were used to evaluate doublet and triplet mutation
150 orders, respectively. When analyzing the percentage of cells with a certain mutation, the
151 denominator was the number of cells with a call for that mutation. Comparisons between
152 mutation order and clinical characteristics were tested with a Wilcoxon rank-sum test unless
153 otherwise specified.

154 To ensure that the data supported the paths between every driver mutation in the same
155 clone, the percent of cells with a later mutation that contained the earlier mutation, the “cell
156 support,” was calculated for each mutation pair. Paths with <50% cell support were “low-
157 support.” Variants in low-support paths were excluded based on how many low-support paths
158 they contributed to and their distal position in the tree (Supplementary Methods, Supplementary
159 Table 3, Supplementary Figure 5).

160

161

162 Results

163 Creating mutation trees

164 Three targeted single-cell AML DNA sequencing datasets were merged (10–12), resulting
165 in 207 patients with AML who had at least two driver mutations, 275 samples, 823 mutation

166 events, and 1 639 162 cells (Supplementary Figure 1). Most samples were cytogenetically normal
167 (53%), and datasets had similar patient demographics but varied in distributions of laboratory
168 values, treatment, and sample availability at diagnosis (Table 1). Although all sequencing panels
169 covered 19 commonly mutated genes, datasets differed in the size of the sequencing panels
170 (Supplementary Table 1), number of cells per sample, and the Tapestry Pipeline allele dropout
171 estimate (Supplementary Figure 6). After aggregating these datasets, mutations were represented
172 in similar proportions as in the TCGA (20) and BeatAML (21) studies, except for enrichment in
173 mutations common in AML, such as in *NPM1* and *FLT3*, and in low-level signaling mutations
174 (Supplementary Figure 7A); for instance, 58% of *KRAS* mutations were in <10% of the
175 corresponding sample's cells.

176 Using SCITE (16,17), we created a mutation tree from each patient's mutation matrix (e.g.
177 Figure 1A). The trees had variable numbers of pathways and genes per pathway (Figure 1B-C),
178 and the most common pairwise links between mutations involved *NPM1*, *DNMT3A*, *FLT3*, *NRAS*,
179 and *IDH2* (Figure 1D). These orderings were corroborated by bulk sequencing since differences
180 in VAF (variant allele frequency) from sequencing done using the same samples and variants
181 correlated with differences in the mutated percentage of cells for pairs of variants in the same
182 clones (Pearson correlation 0.57, $p = 2 \times 10^{-51}$, Supplementary Figure 7B). Of the 101 trees that
183 had branched evolution, signaling mutations represented 66% of the events that immediately
184 followed a branching point (Supplementary Figure 8A). In contrast, *NPM1* mutations frequently
185 served as a branching point (Supplementary Figure 8B) because *NPM1* often preceded signaling
186 mutations; if branching occurred after an *NPM1* mutation, 93% of such occasions involved a
187 signaling mutation vs. 28% if branching did not occur.

188 When summarizing mutations to genes (Figure 1E), 224 distinct evolutionary orderings
189 occurred across all patients (e.g. *DNMT3A*→*NPM1* is indistinct from *DNMT3A*→*NPM1*→*FLT3*).
190 Given the complexity of Figure 1E, we merged trees but summarized events according to the
191 biological pathway corresponding to each gene (Figure 1F, Supplementary Table 2). Mutations
192 related to DNA methylation (e.g. *DNMT3A*, *IDH1/2*) were frequently early, and terminal events
193 were often signaling mutations. We also noted that DNA methylation mutations often followed
194 other DNA methylation mutations, which was driven by specific types of DNA methylation
195 mutations that are less associated with AML progression (22). For example, while *DNMT3A* R882,
196 *IDH1*, and *IDH2* mutations commonly preceded *NPM1* or signaling mutations (Supplementary

197 Figure 9A), *DNMT3A* non-R882 mutations usually preceded other DNA methylation mutations
198 (Supplementary Figure 9B).

199

200 Pairwise mutation co-occurrence and order

201 To further characterize the co-occurrence of mutations, we analyzed the frequency at which
202 mutations occurred in the same or different clones (Figure 2A). Signaling mutations
203 (Supplementary Table 2) in the same cases typically occurred in different clones. For instance,
204 different *NRAS* mutations occurred in distinct clones in 100% of cases. In contrast, *NPM1*
205 mutations nearly always (>90% cases) co-occurred in the same clone as mutations in signaling
206 genes, DNA methylation genes, or transcription factors (Figure 2A).

207 Many mutations also often had characteristic orderings relative to each other, such as
208 *DNMT3A* mutations occurring early and signaling mutations occurring late (Figure 2B,
209 Supplementary Table 4), similar to prior work (8). However, transcription factors like *RUNX1* and
210 *WT1* had variable mutation orderings, appearing both before and after mutations that are typically
211 early (e.g. *DNMT3A*) or late (e.g. *FLT3*).

212 Analyzing the order of mutation trios (rather than pairs) corroborated these findings, where
213 trios often began with DNA methylation mutations and terminated with signaling mutations
214 (Supplementary Table 5). Evolution of *DNMT3A*→*NPM1*→*FLT3* was common, but other
215 mutations trios had variable mutation orderings, like combinations with DNA methylation and
216 splicing mutations.

217

218 Uncommon mutation orders

219 Although many mutation pairs occurred in characteristic orders, we noted several cases
220 where mutation order deviated from typical patterns, such as when signaling mutations occurred
221 before a DNA methylation or *NPM1* mutation (Supplementary Figure 10).

222 Before characterizing these atypical orderings in detail, we validated their presence. First,
223 if signaling mutations came before *NPM1* or DNA methylation mutations, then the percentage of
224 cells with those mutations should be higher. Indeed, the signaling mutation clone size in diagnostic
225 samples was higher when the mutation came before (vs. after) the *NPM1* or DNA methylation
226 mutations ($p = 1.1 \times 10^{-12}$, Figure 3A). Interestingly, the percentage of cells with *NPM1* or DNA
227 methylation mutations was high irrespective of relative signaling mutation order (Figure 3B).

228 Next, if signaling mutations came first, then both the percentage of mutated cells and the bulk VAF
229 should be higher than those of *NPM1* and DNA methylation mutations. Indeed, across all samples
230 and driver mutations, the signaling mutation's percentage of mutated cells and VAF were higher
231 when it was first (89% [51/57] and 63% [15/24] of pairwise comparisons, respectively) and lower
232 when second (94% [318/338] and 93% [140/151]).

233 Although these results corroborated the existence of signaling-first cases, the signaling
234 mutation-only clones in the signaling-first cases were consistently small. Using the difference in
235 percentage of mutated cells as a proxy for clone size, the single-mutant clone size was smaller in
236 signaling-first cases than in *NPM1*/DNA methylation-first cases ($p = 4 \times 10^{-18}$, Figure 3C). This
237 difference was also corroborated using the difference in bulk VAFs as a proxy for single-mutant
238 clone size ($p = 7 \times 10^{-5}$, Figure 3D).

239 A similar pattern of single-mutant clone size was previously seen in *JAK2*-first vs. *TET2*-
240 first MPNs, where *JAK2*-first cases had fewer single-mutant HSPCs, suggesting that *TET2*
241 mutation increased the fitness of *JAK2* mutation in HSPCs (6). Thus, we suspected that *NPM1* and
242 DNA methylation mutations offered a selective advantage for signaling mutations among HSPCs
243 in AML. We explored this phenomenon by examining new mutations across serial samples (25
244 diagnosis/relapse pairs, 15 relapse/relapse pairs, 34 patients, Figure 4A). Most new mutations at
245 relapse were signaling mutations (60%, 21/35), and new signaling mutations tended to arise after
246 a previously present DNA methylation or *NPM1* mutation. When considering all potential nodes
247 in a tree from which signaling mutations could arise (including the possibility of no prior
248 mutations), *NPM1* and DNA methylation mutations disproportionately served as the immediate
249 parent node for a new signaling mutation (9/10 parent nodes, Fisher's test $p = 0.002$). For example,
250 in Figure 4B, the *NRAS* mutations arose in the *DNMT3A* clone, despite the *DNMT3A* mutation
251 being present in 41% of the earlier sample's cells compared to $\geq 90\%$ of cells for the other
252 mutations. Because signaling mutations disproportionately followed DNA methylation and *NPM1*
253 mutations, *NPM1* and DNA methylation mutations may offer an advantage for signaling mutations
254 in HSPCs.

255

256 Clinical correlates with mutation order

257 Because *TET2* mutations change the HSPC balance in MPNs (6), we hypothesized that any
258 advantage conferred by DNA methylation mutations in AML was partially due to expansion of

259 more immature HSPCs, apparent as blasts. To explore this, we compared “late” and “early”
260 mutations, which are those that occur with and without any preceding mutations in the scDNAseq
261 data. Indeed, the bone marrow blast percentage was higher in diagnostic samples with early DNA
262 methylation mutations compared to late DNA methylation mutations ($p = 0.08$, Figure 5A), while
263 the bone marrow granulocyte and monocyte percentages were generally lower ($p = 0.15$ and $p =$
264 0.09 , respectively, Figure 5B-C).

265 In contrast, signaling mutation order (see Supplementary Methods for justification of the
266 “early” and “late” categorization of signaling mutations) was not associated with the bone marrow
267 cell percentages ($p \geq 0.7$ for all comparisons), but it was associated with higher peripheral white
268 blood cell (WBC) counts ($p = 0.099$, Figure 5D). Although peripheral blast counts were higher in
269 signaling-early cases (median 14.8 vs. 3.7, rank-sum $p = 0.14$), so were the peripheral granulocyte
270 and monocyte counts ($p = 0.17$ and $p = 0.089$, respectively, Figure 5E-F). Notably, we consider
271 signaling mutations to be one group for simpler interpretation, but they have different clinical
272 phenotypes, such as early *NRAS/KRAS* mutations having higher monocyte counts than later
273 *NRAS/KRAS* mutations ($p = 0.056$), a trend not seen for *FLT3* mutations ($p = 0.38$).

274 To ensure that these associations between order and cell composition were not dataset-
275 specific, we used proxies for early and late mutation order, specifically high and low VAFs (cutoff
276 0.3, previously used to define dominant and clonal mutations (23,24)), for validation in the
277 BeatAML bulk DNA sequencing data (21). Early DNA methylation mutations were indeed
278 associated with higher bone marrow blast percentages ($p = 0.00041$, Supplementary Figure 11A).
279 In contrast, while early signaling mutations were not associated with bone marrow blast percentage
280 ($p = 0.35$), they were associated with higher peripheral white blood cells, granulocytes, and
281 monocytes ($p < 0.05$ for all comparisons, Supplementary Figure 11B-D).

282 Although these mutation orderings had distinct phenotypes, we also wished to distinguish
283 whether the phenotype was related to the order or the increased clonal burden that resulted from a
284 mutation occurring earlier. Thus, using the scDNAseq data, we performed multiple linear
285 regression adjusting for patient age and the percent of cells with the relevant mutation
286 (Supplementary Table 6). In multivariable analyses, DNA methylation clone size ($p = 0.0079$), but
287 not mutation order ($p = 0.21$), was associated with bone marrow blast percentage, suggesting that
288 clone size mediated the association between DNA methylation order and blast percentage
289 (Supplementary Table 6A). In a similar regression, signaling mutation clone size, rather than
290 mutation order, was significantly associated with peripheral blast percentage ($p = 0.0084$,

291 Supplementary Table 6B). However, signaling mutation order was independently associated with
292 peripheral granulocyte and monocyte counts ($p = 0.088$ and 0.035 , respectively, Supplementary
293 Table 6B), suggesting that the order of signaling mutations, not just the clonal burden, contributed
294 to more mature myeloid cell counts.

295 We next tested whether mutation orderings in AML could explain other patient and disease
296 characteristics, such as younger age and increasing signaling mutation homozygosity, which are
297 associated with *JAK2*-first MPN cases (6). Indeed, in diagnostic samples with early signaling
298 mutations, signaling mutations were more often homozygous (median 5% vs. 21% of cells
299 homozygous, $p = 0.049$, Figure 6A), and patients were younger (median 52 vs. 59 years old, $p =$
300 0.058 , Figure 6C). In contrast, the same patterns did not hold for DNA methylation mutations
301 (Figure 6B,D). Notably, the association with signaling mutation homozygosity was driven by a
302 minority of cases (Figure 6A) and primarily *FLT3* ($p = 0.011$), for which loss of heterozygosity
303 has previously been associated with poor prognosis (25). Although detecting zygosity in
304 scDNAseq data could be confounded by allele dropout, we found no evidence of this since *FLT3*
305 mutation homozygosity was also not correlated with the number of cells missing mutation calls
306 for the relevant mutation or with sample-level allele dropout (Spearman correlation 0.04 [$p = 0.78$]
307 and 0.07 [$p = 0.65$], respectively).

308 This constellation of evolutionary patterns and clinical correlates involving signaling
309 mutations also creates potential to better understand other mutations. For example, *WT1* mutations
310 contribute to relapse (26) but have an unclear role in AML pathogenesis (27), and we found that
311 *WT1* mutations share many characteristics with signaling mutations. Like mutations in *FLT3* and
312 *NRAS*, *WT1* mutations frequently occurred in *NPM1*-mutant clones (Figure 2A, Figure 4A); early
313 *WT1* mutations often occurred in younger patients; and *WT1*-first cases had small single-mutant
314 clones when co-occurring with *NPM1* mutations (Supplementary Figure 12). In multivariable
315 analyses, early *WT1* mutations were also associated with age and higher neutrophil and monocyte
316 counts (Supplementary Table 6C).

317 Although we found several phenotype differences associated with mutation order between
318 DNA methylation and signaling mutations, patients with these different orderings did not have
319 significantly different overall survival (Cox regression age-adjusted $p = 1$ for signaling vs. DNA
320 methylation first). Among relatively prevalent mutation orderings, *SF3B1*→*FLT3* was nearly
321 significantly associated with a worse prognosis after false discovery rate (FDR) correction (age-
322 adjusted hazard ratio 5.6 , q -value = 0.056 , Supplementary Figure 13A). However, this association

323 was no longer significant after adjusting for the presence of an *SF3B1* mutation ($p = 0.44$), which
324 itself carries a poor prognosis (4).

325 Still, exploratory analyses of other phenotypes at diagnosis (Supplementary Figure 13B-E)
326 revealed meaningful associations, such as evolution involving *IDH1/IDH2* mutations and lower
327 granulocyte (median 1.7 vs. 3.0, $p = 3.6 \times 10^{-6}$) and monocyte counts (median 1.2 vs. 1.9, $p =$
328 0.0063), or orderings with *SRSF2* occurring predominantly in older individuals (median age 73 vs.
329 59, $p = 0.017$).

330
331
332

333 Discussion

334 We showed that although AML evolution is heterogeneous, mutations tend to occur in
335 characteristic orders, both at the levels of the genes and the biological pathways involved. This is
336 consistent with prior findings that certain mutations, such as those related to epigenetics, often
337 occur early in evolution whereas signaling mutations occur later (8).

338 However, we expanded on these findings through analysis of large-scale single-cell
339 sequencing data, identifying important patterns in clonal architecture and how those relate to
340 clinical phenotype in AML. We found that many AML cases are characterized by linear
341 evolution, with branching evolution primarily involving signaling mutations. Our analyses also
342 revealed several cases with atypical or poorly characterized mutation orderings, such as signaling
343 mutations preceding DNA methylation mutations or DNA methylation mutations preceding other
344 DNA methylation mutations. Early signaling mutations were associated with 1) proliferative
345 disease, 2) increased signaling mutation homozygosity, and 3) younger patient age. These results
346 are analogous to previous findings in MPNs (6), but we established these conclusions in a more
347 acute, aggressive, and heterogeneous disease. Additionally, the mutation order framework
348 provided insight into poorly understood mutations, like in *WT1*, which had evolutionary patterns
349 and phenotypic associations similar to signaling mutations but where the associations with age
350 and proliferation were independent of the effects of signaling mutations in multiple regression.

351 By using serial samples, we also showed that signaling mutations commonly arise in
352 clones containing mutations in *NPM1* and those related to DNA methylation, suggesting that

353 these mutations may offer a relative fitness advantage for signaling mutations in HSPCs. This
354 was further corroborated by the small clone size of single-mutant clones in signaling-first cases.
355 Because the size of the DNA methylation clones correlated with the bone marrow blast
356 percentage in our scDNAseq dataset and the BeatAML dataset, any advantage may be mediated
357 by a shift to immature cells in the bone marrow.

358 This study has several strengths. First, to our knowledge, this is the largest analysis to
359 date of single-cell DNA sequencing data, an increasingly important data type (28), within a
360 single disease, and the first to benefit from merging multiple clinically relevant datasets together.
361 Second, we leveraged the granular clonal architecture revealed by these data to develop an
362 algorithm to model FLT3-ITD evolution. This is important because the presence of multiple
363 ITDs is associated with a worse prognosis (29), but if multiple ITDs are detected, they may not
364 represent distinct evolutionary events because ITD sequences can be unstable (30) or may be the
365 result of technical artifacts. Third, we used state-of-the-art algorithms to create mutation trees
366 and derive mutation order for each patient's samples, allowing us not only to identify which
367 mutations tend to occur early vs. late but also to identify the order of mutations in a sample.

368 Most importantly, this study adds a new dimension to typical analyses of mutations in
369 AML by examining the order of mutations rather than their presence, co-occurrence, or clonal
370 burden, and this order was associated with clinically relevant traits. Although there is
371 tremendous excitement about how patterns of clonal evolution contribute to the disease course
372 (10–12,28,31), it is crucial to distinguish the effects of clonal architecture from the effects of
373 common clinical measurements that can be derived from bulk sequencing. For example, in some
374 analyses, we found that mutation order itself was independently associated with a phenotype,
375 while in others, we found that the presence of clonal burden of select mutations, rather than the
376 mutation order, mediated association with clinical features. Regardless, considering mutation
377 order will likely be clinically useful, especially when selecting targeted therapies. For example,
378 when *IDH* and *FLT3* mutations co-occur, they virtually always occur in the same clone (Figure
379 2A). Because *IDH* mutations usually come first in evolution (Figure 2B), the cells that have
380 *FLT3* mutations typically also have *IDH* mutations, suggesting that *IDH* could be targeted to
381 treat the *FLT3*-mutant cells. However, if *FLT3* comes first, there could be residual *FLT3*-positive
382 cells if only the *IDH* mutation is targeted.

383 Our study also has some limitations. First, we focus on mutations in individual genes
384 rather than also analyzing large structural rearrangements, which are important in classifying

385 AML (4). Second, this study does not incorporate single-cell surface protein markers (10,12),
386 which may be helpful to distinguish AML cells from other non-leukemic clonal hematopoiesis
387 cells in a sample (32). However, this limitation would not affect the conclusions of this study
388 since many of the mutations analyzed, such as those in *NPM1*, are specific to AML (33) or are
389 uncharacteristic of clonal hematopoiesis. Third, the available data cannot be leveraged to
390 estimate how quickly the AML evolved, unlike recent whole genome sequencing studies focused
391 on MPNs (34,35). However, by using clinical data, we noted that patients whose disease had
392 early signaling mutations were usually younger, suggesting a faster evolution to AML. Fourth,
393 given the lack of single-cell whole-genome sequencing, we cannot rule out that other driver
394 mutations absent from the sequencing panels that are essential for the clonal evolution were
395 excluded. However, this does not invalidate the orderings and overall trends we observed. Lastly,
396 to identify correlations between mutation order and clinical variables, we used retrospective data,
397 and unknown confounders could explain the observed associations.

398 Future studies could model AML evolution in the context of surface protein markers
399 (34,35) or gene expression (36), or with either larger targeted sequencing panels or a larger
400 dataset. It also remains unclear how specific treatments, such as targeted therapies, affect the
401 clonal architecture of AML, and this could be studied more closely.

402 AML is increasingly understood as a heterogeneous disease that evolves from other
403 conditions, such as clonal hematopoiesis and myeloproliferative neoplasms. We foresee a future
404 where treatment is decided not only based on what is observed in a case of the disease, but how
405 that disease came to existence. Modeling the development of AML by placing mutations in their
406 context rather than focusing on the traits of a static sample may open new avenues of both
407 clinical and basic research. These large-scale evolutionary models are a step towards that future.

408

409 Acknowledgements

410 LAM was supported by the National Cancer Institute (NCI) grant R00CA252005. RLB was
411 supported by grant 5R00CA248460 from the NCI. RM was supported by National Institutes of
412 Health (NIH) Grant 1R01CA251331 and the Stanford Ludwig Center for Cancer Stem Cell
413 Research and Medicine. TR was supported by the American Society for Hematology Graduate
414 Hematology Award. MS was supported by the Leukemia & Lymphoma Society Fellow Award,
415 the Chan-Zuckerberg Physician Scientist Award, and the Stanford Biomedical Informatics NLM
416 training grant T15 LM007033-40. AE was supported by the NCI under award F32CA250304,
417 the Advanced Residency Training Program at Stanford, and the American Society of

418 Hematology Scholar Award. BB was supported by the Blavatnik Family Foundation and NIH
419 training grant 5T32CA9302-40. RLL is supported by a Cycle For Survival Innovation Grant,
420 NCI grant R35 CA197594 and the NIH/NCI Cancer Center support grant P30 CA008748. NB
421 and JK were partially supported by SNSF Grant 310030 179518 (<http://www.snf.ch>). KT was
422 supported by the AML/MDS Moonshot Grant from MD Anderson and the Leukemia Lymphoma
423 Society Scholar Award.
424

425 Author Contributions

426 MS, BB, AE, AG, RM, KT, KJ, JK, and NB conceived of the project, designed analyses, and
427 analyzed data. KF, KT, HU, TT, and YS designed sequencing data pipelines and analyzed and
428 processed raw sequencing data. MS aggregated clinical and sequencing data, created figures and
429 tables, implemented analyses, and wrote the initial draft of the manuscript. JK and KJ also
430 implemented analyses for the project and advised on granular aspects of data analyses. LAM,
431 RLL, RL, and TR also designed analyses and assisted with merging datasets. All authors assisted
432 in revising the manuscript.
433
434

435 Competing Interests

436 LAM has received honoraria from Mission Bio and has served on their Speakers' Bureau (2020-
437 2021). RM is on the Advisory Boards of Kodikaz Therapeutic Solutions, Orbital Therapeutics,
438 Pheast Therapeutics, and 858 Therapeutics. RM is a co-founder and equity holder of Pheast
439 Therapeutics, MyeloGene, and Orbital Therapeutics. RLL is on the supervisory board of
440 QIAGEN and is a scientific advisor to Imago, Mission Bio, Syndax, Zentalis, Ajax, Bakx,
441 Auron, Prelude, C4 Therapeutics, and Isoplexis for which he receives equity support. RLL
442 receives research support from Ajax and Abbvie and has consulted for Incyte, Janssen,
443 Morphosys, and Novartis. RLL has received honoraria from Astra Zeneca and Kura for invited
444 lectures and from Gilead for grant reviews. KT has received honoraria from Mission Bio and
445 Illumina Inc. and received scientific advisory fees from Symbio Pharmaceuticals.
446
447
448
449

450 Data Availability Statement

451 Genomic data that were created for this study are available on dbGaP with accession
452 phs002049.v1.p1 and, on Sequence Read Archive with NCBI BioProject ID PRJNA648656.
453 Data from Stanford is being submitted to dbGaP. Clinical data are available on request. Code is
454 on Github at <https://github.com/mattschwede/aml-mutation-order>.
455

456 References

- 457
458 1. SEER [Internet]. [cited 2020 Sep 26]. Acute Myeloid Leukemia - Cancer Stat Facts.
459 Available from: <https://seer.cancer.gov/statfacts/html/amyl.html>
- 460 2. Klco JM, Spencer DH, Miller CA, Griffith M, Lamprecht TL, O’Laughlin M, et al.
461 Functional heterogeneity of genetically defined subclones in acute myeloid leukemia. *Cancer*
462 *Cell*. 2014 Mar 17;25(3):379–92.
- 463 3. Quek L, David MD, Kennedy A, Metzner M, Amatangelo M, Shih A, et al. Clonal
464 heterogeneity of acute myeloid leukemia treated with the IDH2 inhibitor enasidenib. *Nat*
465 *Med*. 2018;24(8):1167–77.
- 466 4. Döhner H, Wei AH, Appelbaum FR, Craddock C, DiNardo CD, Dombret H, et al. Diagnosis
467 and management of AML in adults: 2022 recommendations from an international expert
468 panel on behalf of the ELN. *Blood*. 2022 Sep 22;140(12):1345–77.
- 469 5. Papaemmanuil E, Gerstung M, Bullinger L, Gaidzik VI, Paschka P, Roberts ND, et al.
470 Genomic Classification and Prognosis in Acute Myeloid Leukemia. *N Engl J Med*. 2016 Jun
471 9;374(23):2209–21.
- 472 6. Ortman CA, Kent DG, Nangalia J, Silber Y, Wedge DC, Griffin J, et al. Effect of
473 mutation order on myeloproliferative neoplasms. *N Engl J Med*. 2015 Feb 12;372(7):601–12.
- 474 7. Nagata Y, Makishima H, Kerr CM, Przychodzen BP, Aly M, Goyal A, et al. Invariant
475 patterns of clonal succession determine specific clinical features of myelodysplastic
476 syndromes. *Nat Commun* [Internet]. 2019 Nov 26 [cited 2020 Oct 4];10. Available from:
477 <https://www.ncbi.nlm.nih.gov/pmc/articles/PMC6879617/>
- 478 8. Corces-Zimmerman MR, Hong WJ, Weissman IL, Medeiros BC, Majeti R. Preleukemic
479 mutations in human acute myeloid leukemia affect epigenetic regulators and persist in
480 remission. *Proc Natl Acad Sci U S A*. 2014 Feb 18;111(7):2548–53.
- 481 9. Shlush LI, Zandi S, Mitchell A, Chen WC, Brandwein JM, Gupta V, et al. Identification of
482 pre-leukaemic haematopoietic stem cells in acute leukaemia. *Nature*. 2014 Feb
483 20;506(7488):328–33.
- 484 10. Morita K, Wang F, Jahn K, Hu T, Tanaka T, Sasaki Y, et al. Clonal evolution of acute
485 myeloid leukemia revealed by high-throughput single-cell genomics. *Nat Commun*. 2020
486 21;11(1):5327.
- 487 11. Ediriwickrema A, Aleshin A, Reiter JG, Corces MR, Köhnke T, Stafford M, et al. Single-cell
488 mutational profiling enhances the clinical evaluation of AML MRD. *Blood Adv*. 2020
489 10;4(5):943–52.

- 490 12. Miles LA, Bowman RL, Merlinsky TR, Csete IS, Ooi AT, Durruthy-Durruthy R, et al.
491 Single-cell mutation analysis of clonal evolution in myeloid malignancies. *Nature*. 2020 Oct
492 28;1–6.
- 493 13. Poplin R, Ruano-Rubio V, DePristo MA, Fennell TJ, Carneiro MO, Auwera GAV der, et al.
494 Scaling accurate genetic variant discovery to tens of thousands of samples. *bioRxiv*
495 [Internet]. 2018; Available from: <https://www.biorxiv.org/content/early/2018/07/24/2011178>
- 496 14. Morita K, Kantarjian HM, Wang F, Yan Y, Bueso-Ramos C, Sasaki K, et al. Clearance of
497 Somatic Mutations at Remission and the Risk of Relapse in Acute Myeloid Leukemia. *J Clin*
498 *Oncol Off J Am Soc Clin Oncol*. 2018 Jun 20;36(18):1788–97.
- 499 15. Papaemmanuil E, Gerstung M, Malcovati L, Tauro S, Gundem G, Van Loo P, et al. Clinical
500 and biological implications of driver mutations in myelodysplastic syndromes. *Blood*. 2013
501 Nov 21;122(22):3616–27; quiz 3699.
- 502 16. Jahn K, Kuipers J, Beerenwinkel N. Tree inference for single-cell data. *Genome Biol*. 2016
503 May 5;17(1):86.
- 504 17. Kuipers J, Jahn K, Raphael BJ, Beerenwinkel N. Single-cell sequencing data reveal
505 widespread recurrence and loss of mutational hits in the life histories of tumors. *Genome*
506 *Res*. 2017 Nov;27(11):1885–94.
- 507 18. Csardi G, Nepusz T. The igraph software package for complex network research.
508 *InterJournal*. 2006;Complex Systems:1695.
- 509 19. Read TRC, Cressie NAC. Goodness-of-Fit Statistics for Discrete Multivariate Data
510 [Internet]. Springer New York; 1988. (Springer Series in Statistics). Available from:
511 https://books.google.com/books?id=_ce8QgAACAAJ
- 512 20. The Cancer Genome Atlas Research Network. Genomic and Epigenomic Landscapes of
513 Adult De Novo Acute Myeloid Leukemia. <https://doi.org/10.1056/NEJMoa1301689>
514 [Internet]. 2013 May 29 [cited 2021 Mar 12]; Available from:
515 <https://www.nejm.org/doi/10.1056/NEJMoa1301689>
- 516 21. Bottomly D, Long N, Schultz AR, Kurtz SE, Tognon CE, Johnson K, et al. Integrative
517 analysis of drug response and clinical outcome in acute myeloid leukemia. *Cancer Cell*. 2022
518 Aug 8;40(8):850-864.e9.
- 519 22. Jawad M, Afkhami M, Ding Y, Zhang X, Li P, Young K, et al. DNMT3A R882 Mutations
520 Confer Unique Clinicopathologic Features in MDS Including a High Risk of AML
521 Transformation. *Front Oncol*. 2022 Feb 28;12:849376.
- 522 23. Fowler JC, King C, Bryant C, Hall M, Sood R, Ong SH, et al. Selection of oncogenic mutant
523 clones in normal human skin varies with body site. *Cancer Discov*. 2021 Feb 1;11(2):340–
524 61.

- 525 24. Mims AS, Kohlschmidt J, Borate U, Blachly JS, Orwick S, Eisfeld AK, et al. A precision
526 medicine classification for treatment of acute myeloid leukemia in older patients. *J Hematol*
527 *Oncol* *J Hematol Oncol*. 2021 Jun 23;14(1):96.
- 528 25. Whitman SP, Archer KJ, Feng L, Baldus C, Becknell B, Carlson BD, et al. Absence of the
529 wild-type allele predicts poor prognosis in adult de novo acute myeloid leukemia with
530 normal cytogenetics and the internal tandem duplication of FLT3: a cancer and leukemia
531 group B study. *Cancer Res*. 2001 Oct 1;61(19):7233–9.
- 532 26. El Hussein S, DiNardo CD, Takahashi K, Khoury JD, Fang H, Furudate K, et al. Acquired
533 WT1 mutations contribute to relapse of NPM1-mutated acute myeloid leukemia following
534 allogeneic hematopoietic stem cell transplant. *Bone Marrow Transplant*. 2022
535 Mar;57(3):370–6.
- 536 27. Rampal R, Figueroa ME. Wilms tumor 1 mutations in the pathogenesis of acute myeloid
537 leukemia. *Haematologica*. 2016 Jun;101(6):672–9.
- 538 28. Ediriwickrema A, Gentles AJ, Majeti R. Single-cell genomics in AML: extending the
539 frontiers of AML research. *Blood*. 2023 Jan 26;141(4):345–55.
- 540 29. Schranz K, Hubmann M, Harin E, Vosberg S, Herold T, Metzeler KH, et al. Clonal
541 heterogeneity of FLT3-ITD detected by high-throughput amplicon sequencing correlates
542 with adverse prognosis in acute myeloid leukemia. *Oncotarget*. 2018 Jul 10;9(53):30128–45.
- 543 30. Kottaridis PD, Gale RE, Langabeer SE, Frew ME, Bowen DT, Linch DC. Studies of FLT3
544 mutations in paired presentation and relapse samples from patients with acute myeloid
545 leukemia: implications for the role of FLT3 mutations in leukemogenesis, minimal residual
546 disease detection, and possible therapy with FLT3 inhibitors. *Blood*. 2002 Oct
547 1;100(7):2393–8.
- 548 31. Benard BA, Leak LB, Azizi A, Thomas D, Gentles AJ, Majeti R. Clonal architecture predicts
549 clinical outcomes and drug sensitivity in acute myeloid leukemia. *Nat Commun*. 2021 Dec
550 13;12(1):7244.
- 551 32. Dillon LW, Ghannam J, Nosiri C, Gui G, Goswami M, Calvo KR, et al. Personalized Single-
552 Cell Proteogenomics to Distinguish Acute Myeloid Leukemia from Non-Malignant Clonal
553 Hematopoiesis. *Blood Cancer Discov*. 2021 Jul;2(4):319–25.
- 554 33. Chen Y, Hu J. Nucleophosmin1 (NPM1) abnormality in hematologic malignancies, and
555 therapeutic targeting of mutant NPM1 in acute myeloid leukemia. *Ther Adv Hematol*. 2020
556 Feb 3;11:2040620719899818.
- 557 34. Fabre MA, de Almeida JG, Fiorillo E, Mitchell E, Damaskou A, Rak J, et al. The
558 longitudinal dynamics and natural history of clonal haematopoiesis. *Nature*. 2022
559 Jun;606(7913):335–42.
- 560 35. Williams N, Lee J, Mitchell E, Moore L, Baxter EJ, Hewinson J, et al. Life histories of
561 myeloproliferative neoplasms inferred from phylogenies. *Nature*. 2022 Feb;602(7895):162–
562 8.

563 36. van Galen P, Hovestadt V, Wadsworth M, Hughes T, Griffin GK, Battaglia S, et al. Single-
564 cell RNA-seq reveals AML hierarchies relevant to disease progression and immunity. *Cell*.
565 2019 Mar 7;176(6):1265-1281.e24.

566 37. Benjamini Y, Hochberg Y. Controlling the False Discovery Rate: A Practical and Powerful
567 Approach to Multiple Testing. *J R Stat Soc Ser B Methodol*. 1995;57(1):289–300.

568

569

570

571 Figure and table legends

572

573 Tables legends

574

575 Table 1: Characteristics of patients from each dataset either as a proportion of the dataset or as a
576 median and a range. *Only diagnostic samples used for these variables.

577

578 Figures legends

579 Figure 1: A) Example tree. Distributions of B) the number of distinct evolutionary pathways per
580 tree (number of trees = 207), and C) the average number of mutations per pathway. D) Most
581 common two-gene evolutionary pathways mutated, when mutations were summarized by gene.
582 E) All trees merged, summarized by the gene in which the mutation is present, where size of
583 node represents the number of times a particular pathway occurs, starting from the root node.
584 Colors correspond to mutations, where genes with similar functions have similar colors (e.g. blue
585 shades for DNA methylation and red/orange shades for signaling mutations). F) All trees
586 merged, where the mutation events were summarized by pathway, and only evolutionary
587 pathways with at least five events are depicted.

588

589 Figure 2: A) Plot showing whether two mutations occur in the same or different clone,
590 summarized by gene. Size of each dot represents the number of times mutations in two genes
591 occur in the same patient sample, and color represents the frequency they are in the same clone.
592 B) Whether one mutation occurs before another mutation. Size of dot represents the number of
593 times they are in the same clone (not just in the same patient sample), and color represents the
594 proportion of times a mutation in a gene on the y-axis came before a mutation in a gene on the x-
595 axis.

596

597 Figure 3: Boxplots showing the A) percentage of mutated cells containing a signaling mutation
598 vs. whether the signaling mutation came before (First) or after (Second) an *NPM1* or DNA
599 methylation mutation. B) Same plot as (A) except that the focus is on the *NPM1* or DNA
600 methylation mutation percent cells mutated. C) Size of a single-mutant clone stratified by which
601 mutation came first. Single-mutant clone size was estimated by subtracting the proportion of
602 cells with each mutation after removing cells where there was no call for the mutation. This plot
603 shows that the single-mutant clones for *NPM1*/DNA methylation-first cases were higher than in
604 signaling-first cases. D) Difference in variant allele frequency (VAF) using bulk sequencing data
605 from the same samples and variants. In A) and B), only diagnostic samples were used since the
606 absolute amount of disease may vary with treatment, and the $n = 148$ for *NPM1*/DNA
607 methylation-first and $n = 23$ for signaling-first. In C) and D), since the focus was on relative
608 sizes of clones, all samples were used, with $n = 338$ and $n = 57$ for *NPM1*/DNA methylation-first
609 and signaling-first groups, respectively, and because of missing bulk sequencing data in D), $n =$
610 151 and $n = 24$, respectively.

611
612 Figure 4 : A) All new pathways at relapse across all available paired serial samples in the single-
613 cell dataset (derived from 25 diagnosis/relapse and 15 relapse/relapse pairs, 34 patients total).
614 The top layer of events represents events present in the prior sample, although not necessarily the
615 initial event of a tree, and the lower layers represent events gained on a subsequent sample.
616 Genes with more than one instance are labeled directly. B) Example tree for which serial samples
617 are available, where the events circled in yellow are new events on a subsequent sample.

618
619
620 Figure 5: Earlier DNA methylation mutations were associated with higher bone marrow blast
621 percentages while earlier signaling mutations were associated with higher peripheral myeloid
622 cell counts. A-C) Distributions of A) bone marrow blast percentage, B) bone marrow
623 granulocyte percentage, and C) bone marrow monocyte percentage compared to whether a DNA
624 methylation mutation was early, late, or not present in the sample. D-F) Distributions of D) log
625 peripheral blast count, E) log peripheral granulocyte count, and F) log peripheral monocyte count
626 compared to whether a signaling mutation was early, late, or not present.

627
628 Figure 6: Signaling mutation (A-B) zygosity and patient age (C-D) at diagnosis compared to
629 whether signaling (A, C) and DNA methylation (B, D) mutations were early or late (or there was
630 no mutation, in the age comparison) among diagnostic samples. “Early” means that no mutations
631 are known to occur before it based on the scDNAseq dataset.

632
633

634 Supplementary table legends

635

636 Supplementary Table 1: Panels used for sequencing in each respective study.

637

638 Supplementary Table 2: Genes and their corresponding biological pathways used for analysis.

639

640 Supplementary Table 3: Connections in each tree that are poorly supported, specifically that
641 <50% cells with later mutation contain early mutation.

642

643 Supplementary Table 4: Table showing whether one mutation tends to occur before another,
644 among mutations occurring in the same clones and with mutations summarized to genes. P-
645 values were derived using a binomial test and adjusted to Q-values using the Benjamini-
646 Hochberg method (37).

647

648 Supplementary Table 5: Triplet mutation orderings. A trio of mutations was considered for
649 ordering analysis if more than two patients had the three mutations in the same clone. P-values
650 were derived from the exact multinomial test, except for when the binomial coefficient was
651 greater than 10^6 , in which case a Monte Carlo approach was used. Both the number of clones
652 with the three mutations (“Number clones”) and the number of clones with the most common
653 ordering (“Ordering count”) are shown. P-values were calculated both at the A) gene level and
654 B) pathway level and were adjusted using the Benjamini-Hochberg method (37).

655

656 Supplementary Table 6: Multivariable regression analyses. A) Linear regression of DNA
657 methylation mutation order compared to bone marrow blast, granulocyte, and monocyte

658 percentages, before and after adjusting for patient age and DNA methylation mutation burden (%
659 mutated cells). B) Similar regressions as in (A), but predictor variable is signaling mutation order
660 instead of DNA methylation mutation order, and response variable is peripheral white blood cell,
661 granulocyte, and monocyte counts. C) *WT1* mutation order at diagnosis vs. patient age, adjusting
662 for signaling mutation order.

663

664 Supplementary Table 7: Variants from whole exome or extended targeted sequencing data from
665 17 cases with signaling mutations first that would have met criteria for inclusion in this study but
666 were missed on the sequencing panel.

667

668

669 Supplementary table legends

670

671 Supplementary Figure 1: Diagram showing studies included in the analysis, including number of
672 patients and samples from Stanford, MD Anderson, and Memorial Sloan Kettering (MSK).

673

674 Supplementary Figure 2: Number of additional driver mutations discovered on manual review of
675 variants that were initially of unknown significance, stratified by gene.

676

677 Supplementary Figure 3: Plots showing statistics about variants. A) Number of unique driver
678 mutations, variants of unknown significance (VUS), and variants that were excluded
679 (blacklisted) because they were not known to be associated with AML and either 1. occurred in
680 most patients (Excluded – recurrent) or 2. occurred repeatedly in less than 5% of cells (Excluded
681 – low level). B) Source of different types of variants broken down by dataset. C) Distribution of
682 the number of events per driver mutation (where FLT3-ITD is considered a single type of driver
683 mutation), or D) per blacklisted variant.

684

685 Supplementary Figure 4: A) Number of FLT3-ITDs per sample across each dataset. P-value was
686 calculated with a Kruskal-Wallis test. Total ITDs = 151, and total patients = 58. B) Number of
687 FLT3-ITD variants that result with different types of merging strategies (see Supplementary
688 Methods). C) The number of cases that underwent different merging strategies based on our
689 algorithm for choosing a merging strategy. D) The reasons for merging across all cases, where
690 “Max connection support” means that the tree minimized low-support connections, “Same clonal
691 evolution” means that all ITDs were terminal events in the tree and had the same parent event,
692 and “One ITD” means either there was only one ITD or that the sequence of all ITDs were
693 subsequences of another ITD.

694

695 Supplementary Figure 5: After low-support connections were identified in a tree (<50% cells
696 with the later mutation also contained the earlier mutation), mutations were excluded either
697 because they contributed to the most low support connections or were more distal in the tree
698 (Supplementary Methods). A) Bar plot of the number of variants excluded per gene because of
699 low support, across the entire dataset. B) Distribution of proportion of cells mutated among those
700 excluded variants. C) An example tree with a low-support connection (NRAS → KRAS).

701

702

703 Supplementary Figure 6: A) Allele dropout estimate and B) number of cells per sample stratified
704 by dataset and sequencing panel. Stanford and the “MDA 19-gene panel” are the same Mission

705 Bio sequencing panels at different institutions. The “MDA custom panel” is a 37-gene panel
706 created by collaborators at MD Anderson, and “MSK” refers to the 31-gene panel created by
707 collaborators at Memorial Sloan Kettering. P-values were calculated with the Kruskal-Wallis
708 test.

709
710 Supplementary Figure 7: A) Distribution of mutations across different datasets. The top plot is
711 from the current study, second plot from the most recent BeatAML study ¹¹, and third plot from
712 The Cancer Genome Atlas ¹² study. “Subclonal” means that the mutation was present in < 10%
713 of cells. B) Comparison of the difference in percentage of cells mutated in single-cell data and
714 the difference in variant allele frequency (VAF), which is a proxy for the number of cells
715 mutated, in bulk sequencing data. The line represents the predicted association between these
716 values if all variants were heterozygous. Plot B) was created using all available bulk sequencing
717 data from the samples and variants in the single cell data, a total of 577 pairwise comparisons,
718 377 variants, and 139 patients.

719
720 Supplementary Figure 8: A) Percent of mutation events for that gene that immediately follow a
721 branch point, ordered by this percentage. Signaling mutations mostly follow branch points while
722 others generally do not. B) Percentage of times a gene’s mutations serve as a branching point.
723 NPM1 mutations most commonly serve as branching points in evolution, largely because they
724 often immediately precede signaling mutations.

725
726 Supplementary Figure 9: A) Percentage of mutations that immediately followed either DNMT3A
727 R882 or IDH1/2 mutations. B) Percentage of mutations that immediately followed non-R882
728 DNMT3A mutations vs. IDH1/2 mutations. P-values calculated with Fisher’s exact test.

729
730 Supplementary Figure 10: Considering all cases where a signaling mutation preceded another
731 mutation (n = 39), sub-trees were created using the signaling mutation as the starting node, and
732 all such sub-trees were merged. This figure shows what mutations tend to follow signaling
733 mutations, and they are predominantly NPM1 and DNA methylation mutations, although many
734 transcription factor mutations (primarily in WT1) also commonly followed different signaling
735 mutations.

736
737
738 Supplementary Figure 11: Using the BeatAML data ¹¹, A) distribution of bone marrow blast
739 percentage compared to whether DNA methylation mutations were early, late, or absent. B-D)
740 Similar plots comparing signaling mutations to B) log peripheral white blood cell count, C) log
741 peripheral granulocyte counts, and D) log peripheral monocyte counts. Using these bulk
742 sequencing, early and late were defined as VAF (variant allele frequency) ≥ 0.3 or < 0.3 ,
743 respectively.

744
745 Supplementary Figure 12: A) Single-mutant proportions for WT1-first cases and NPM1-first
746 cases. B) Similar comparison using variant allele frequency (VAF) differences between NPM1
747 and WT1 from bulk sequencing using the same variants and samples. A) Early, late, or no WT1
748 mutation at diagnosis compared to age.

749

750
751 Supplementary Figure 13: Pairwise mutation orderings compared to different distributions of
752 clinical variables, specifically A) hazard ratio of overall survival, B) age, C) peripheral blood log
753 blasts), D) peripheral blood log neutrophils, and E) peripheral blood log monocytes compared to
754 all patients without that pairwise path.
755 Supplementary Figure 14: Fraction of trees in the posterior distribution that are identical to the
756 final tree used in the analysis. Generally, the posterior distribution was dominated by one tree.
757
758 Supplementary Figure 15: Extreme example of the consequences of merging FLT3-ITD variants
759 using case AML-88 from the MD Anderson dataset. In this case, A) merging all variants resulted
760 in the FLT-ITD variant to be higher in the tree than with B) conservative merging. However, the
761 FLT3-ITD variant ultimately could not be used because it contributed to too many low support-
762 connections, result in C) the final tree.
763
764 Supplementary Figure 16: Distance of FLT3-ITD variants from root node to the variant when a
765 conservative ITD merging strategy is used (light red) or all ITD variants are merged (blue,
766 becomes purple when mixed with light red in figure). This shows that when merging ITD
767 variants, the more distal ITD variants in the tree are most affected.
768

Figure 1

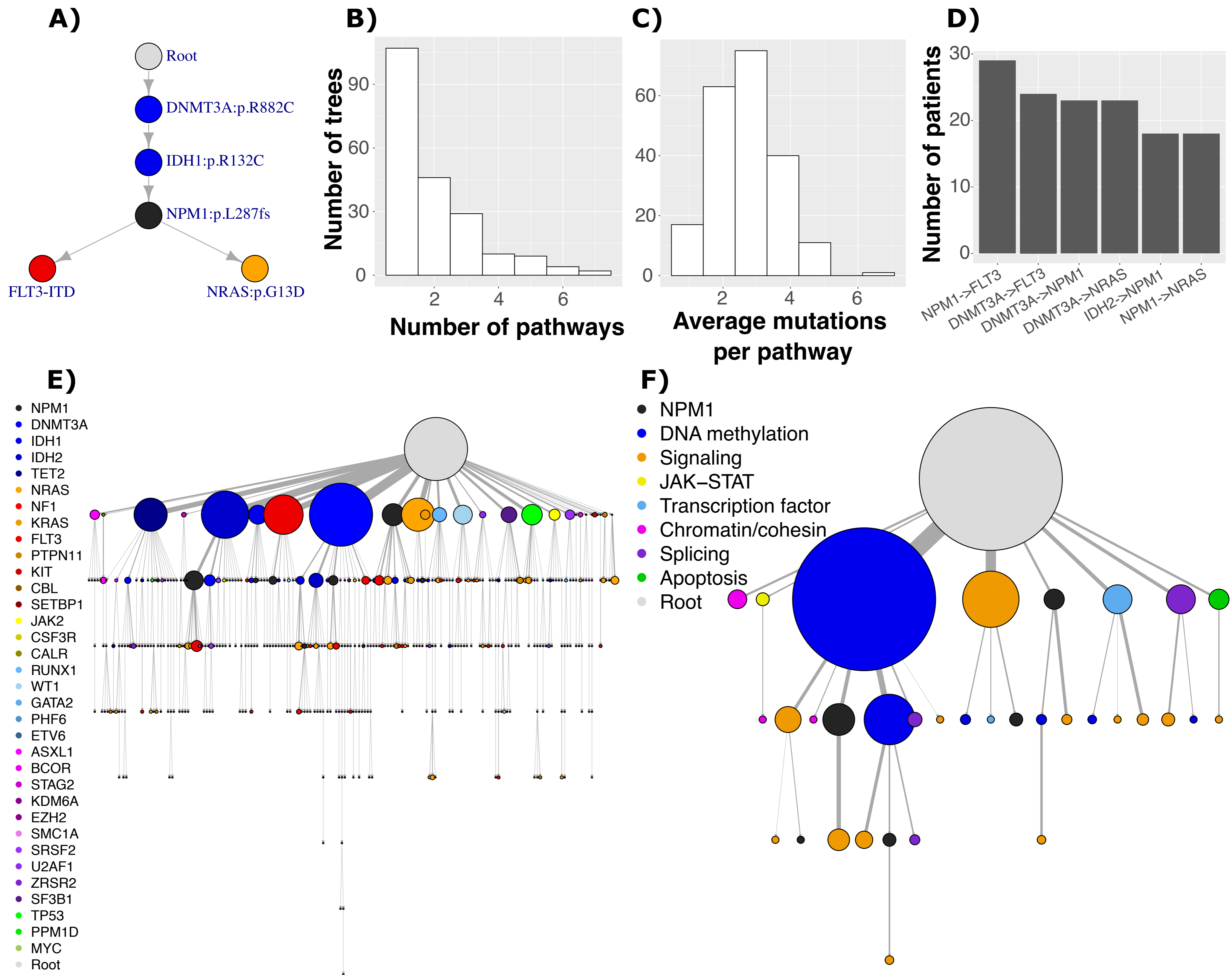
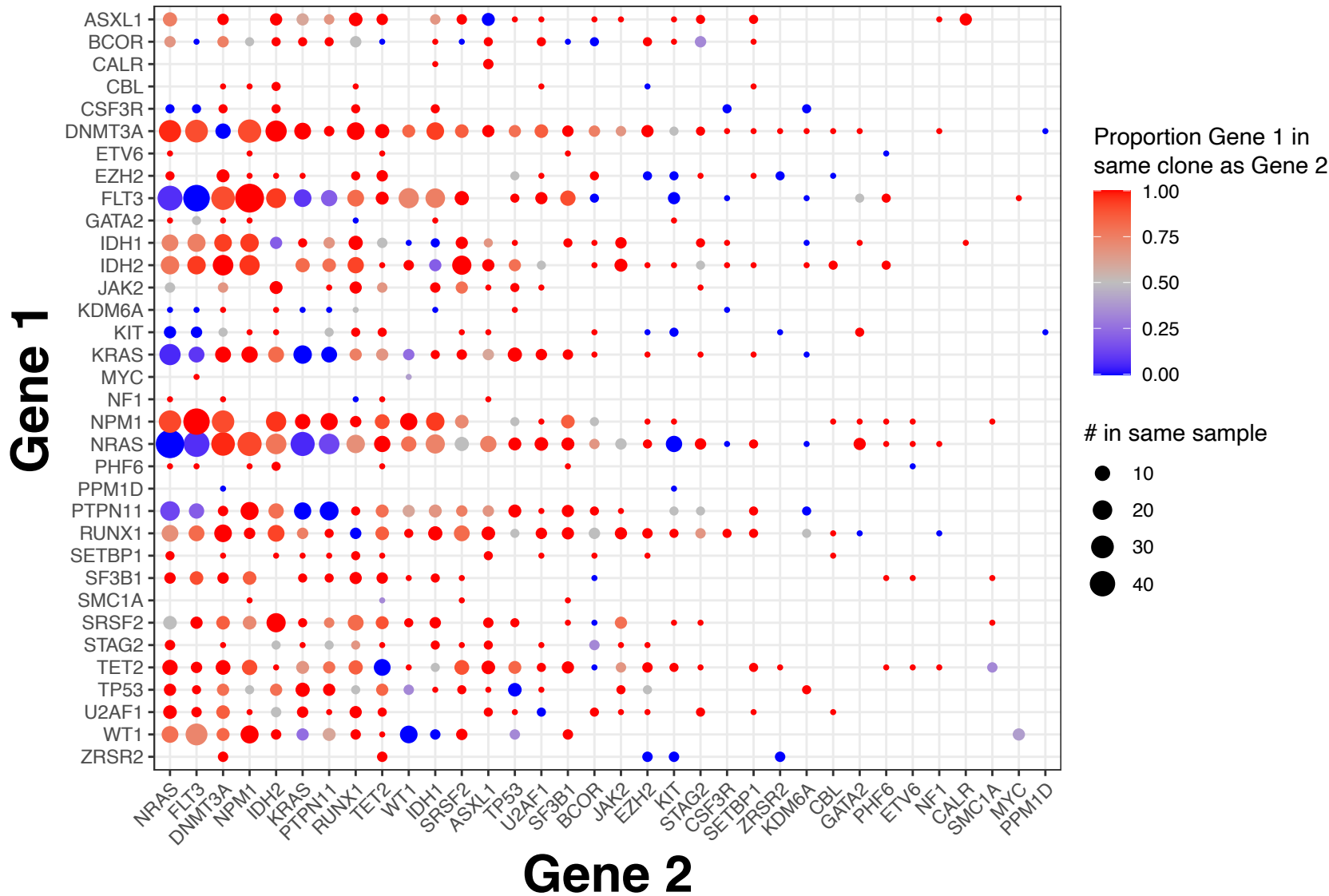


Figure 2

A)



B)

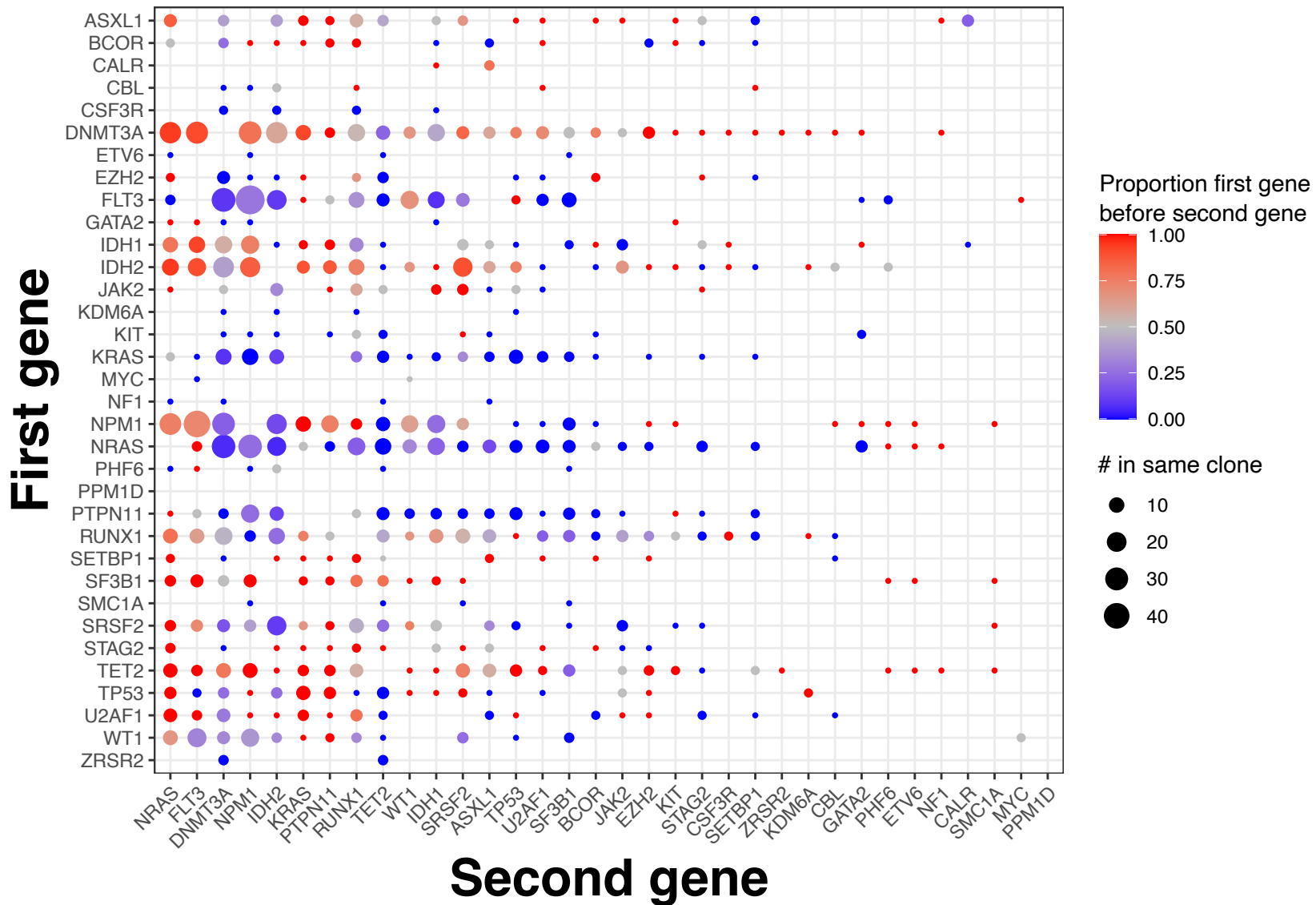


Figure 3

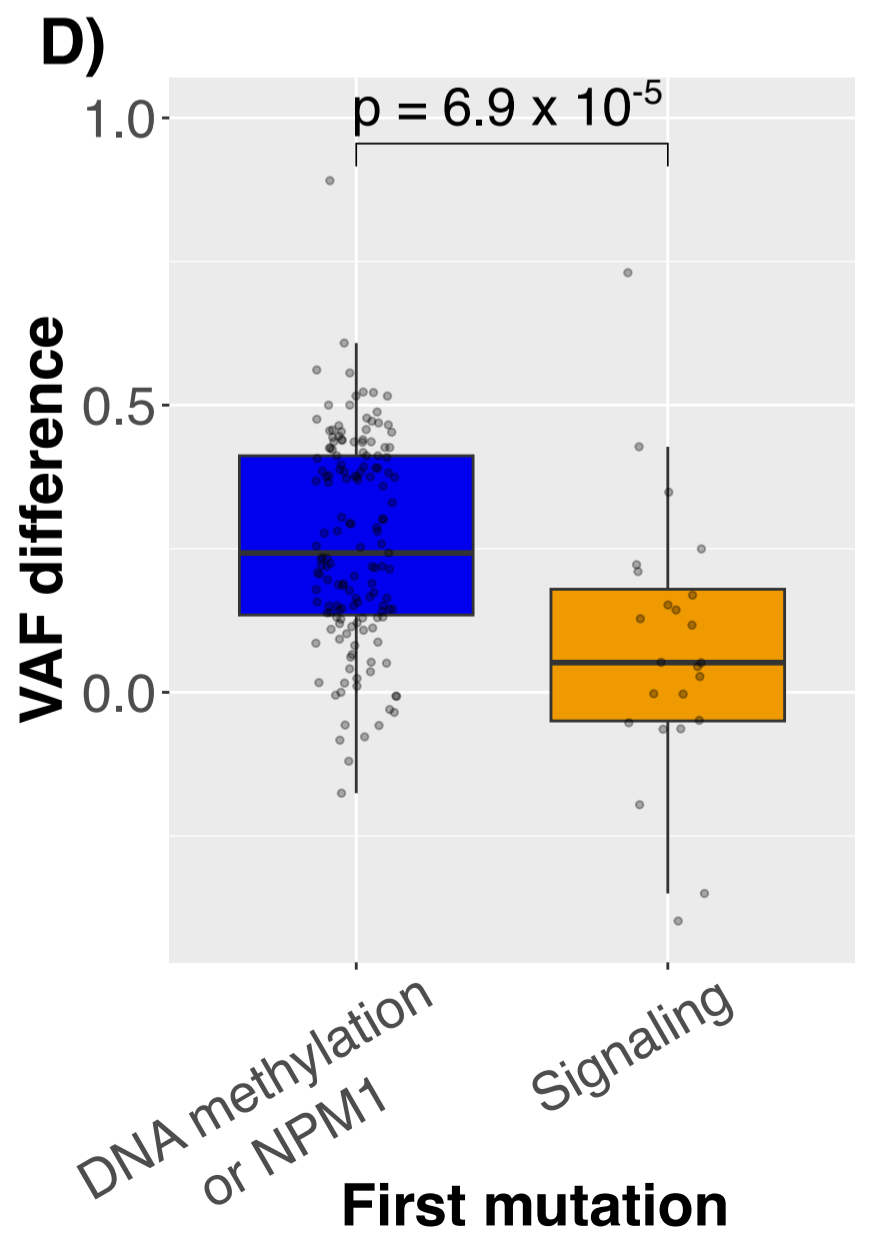
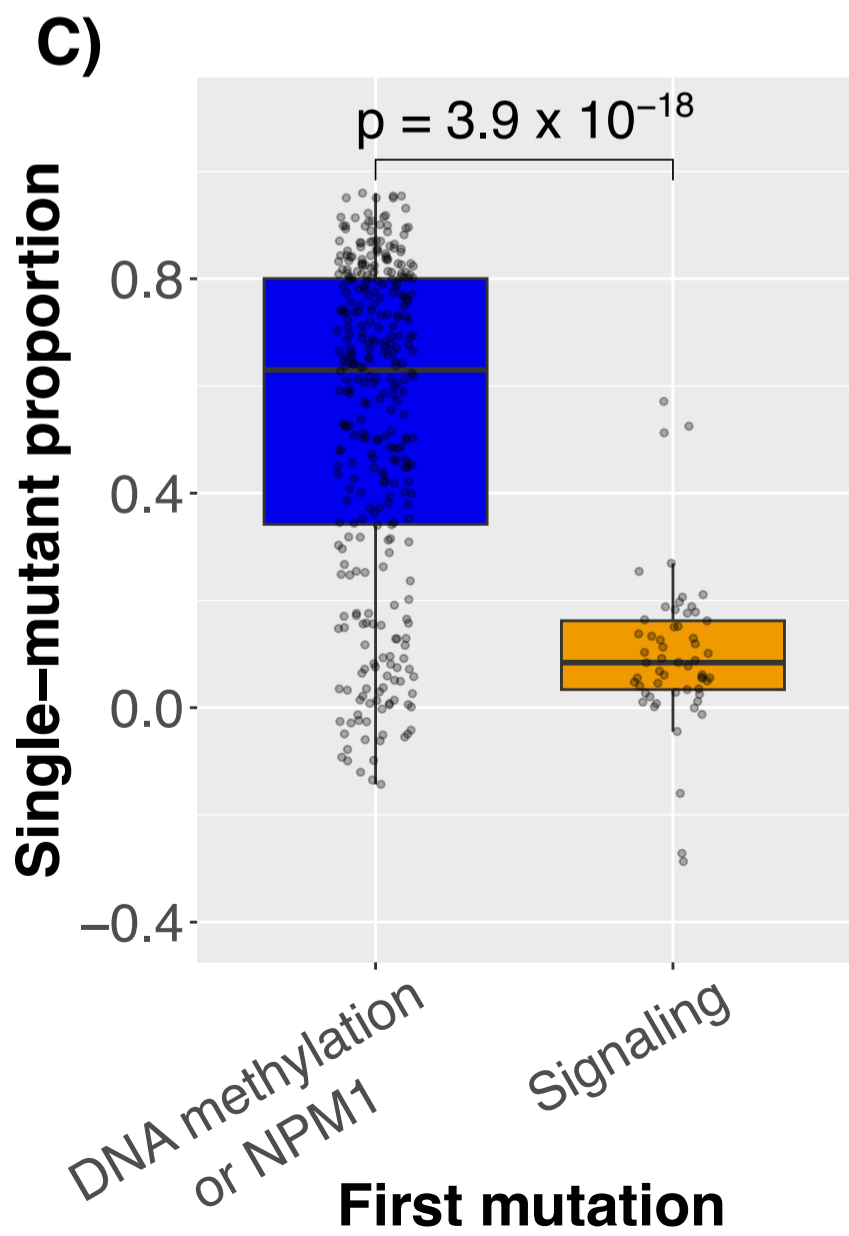
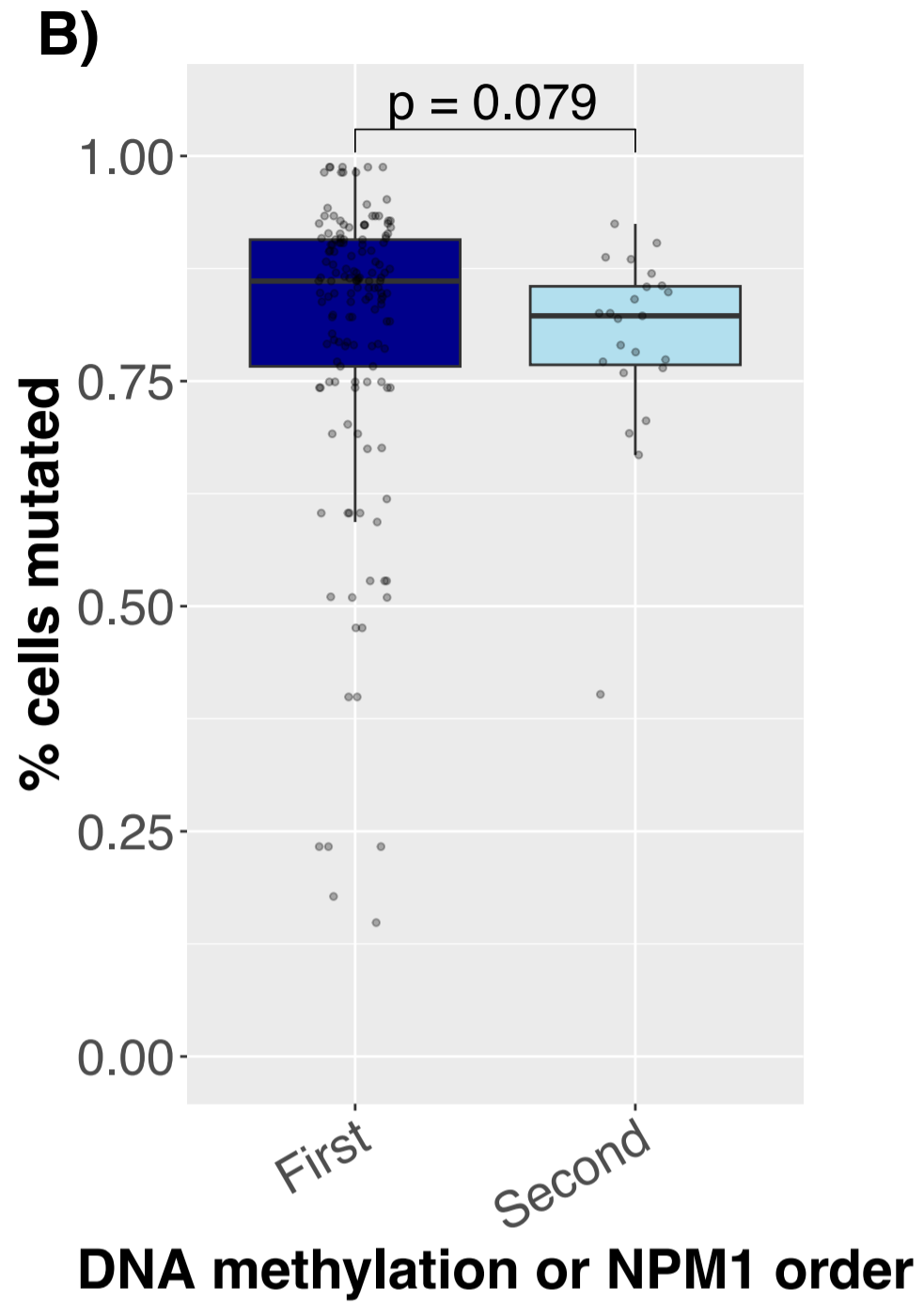
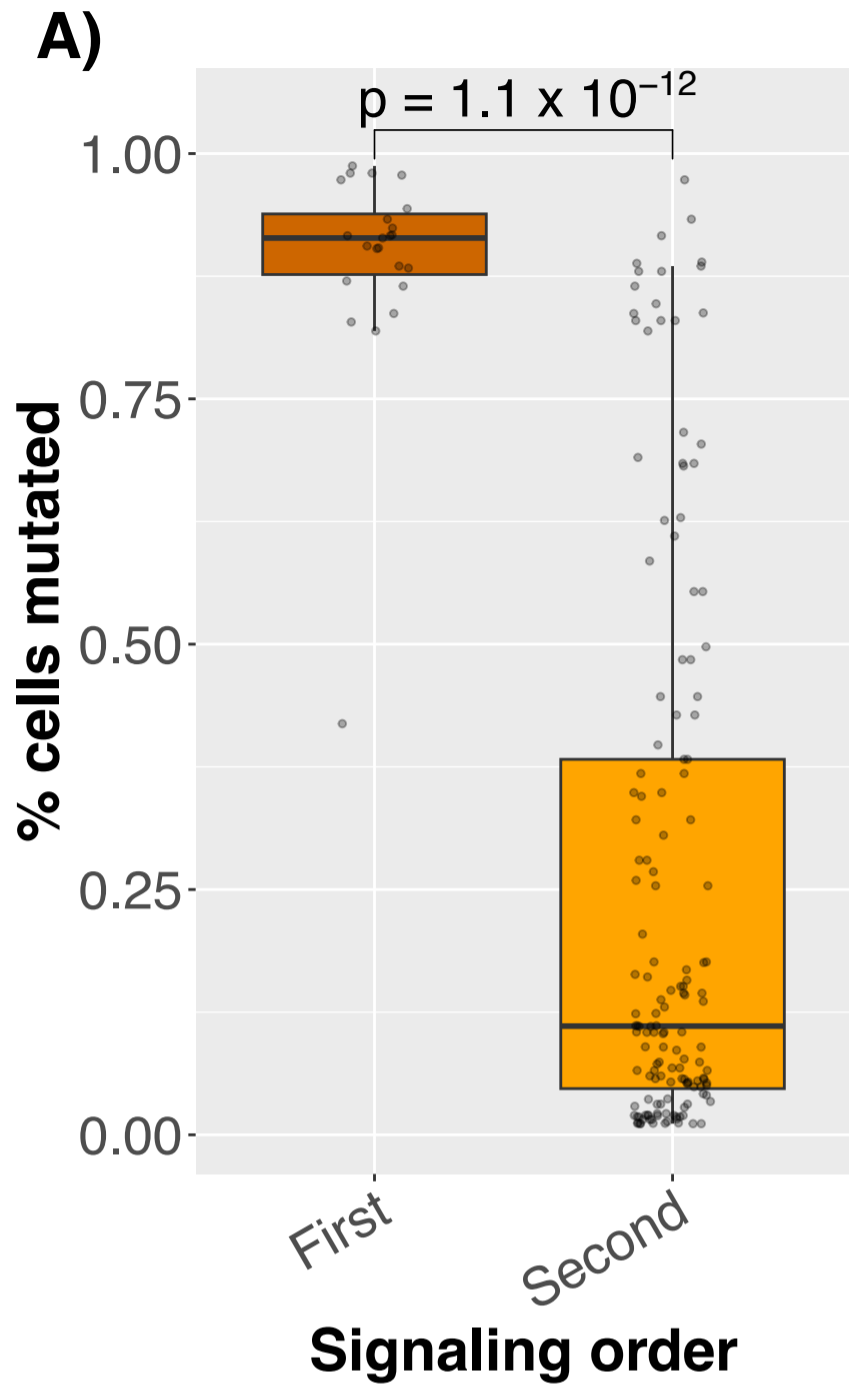
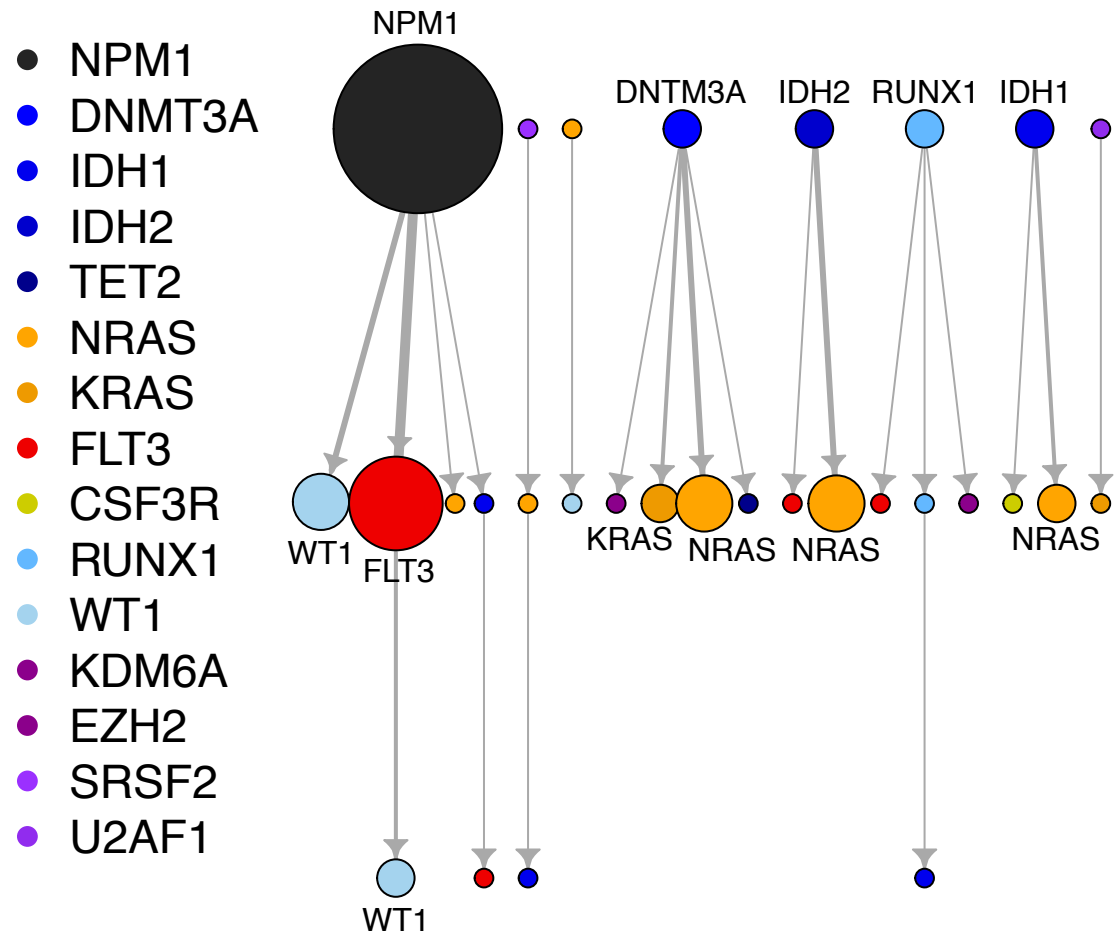


Figure 4

A)



B)

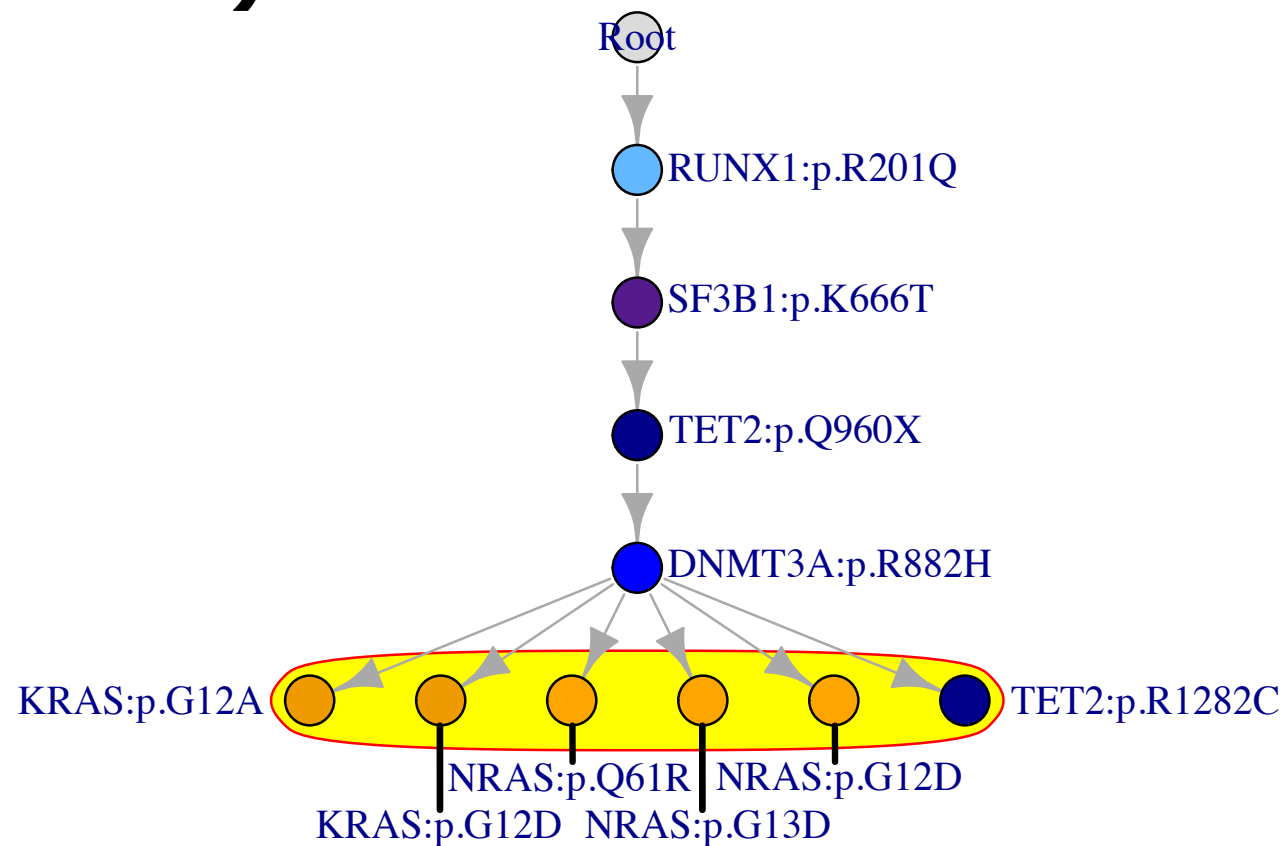
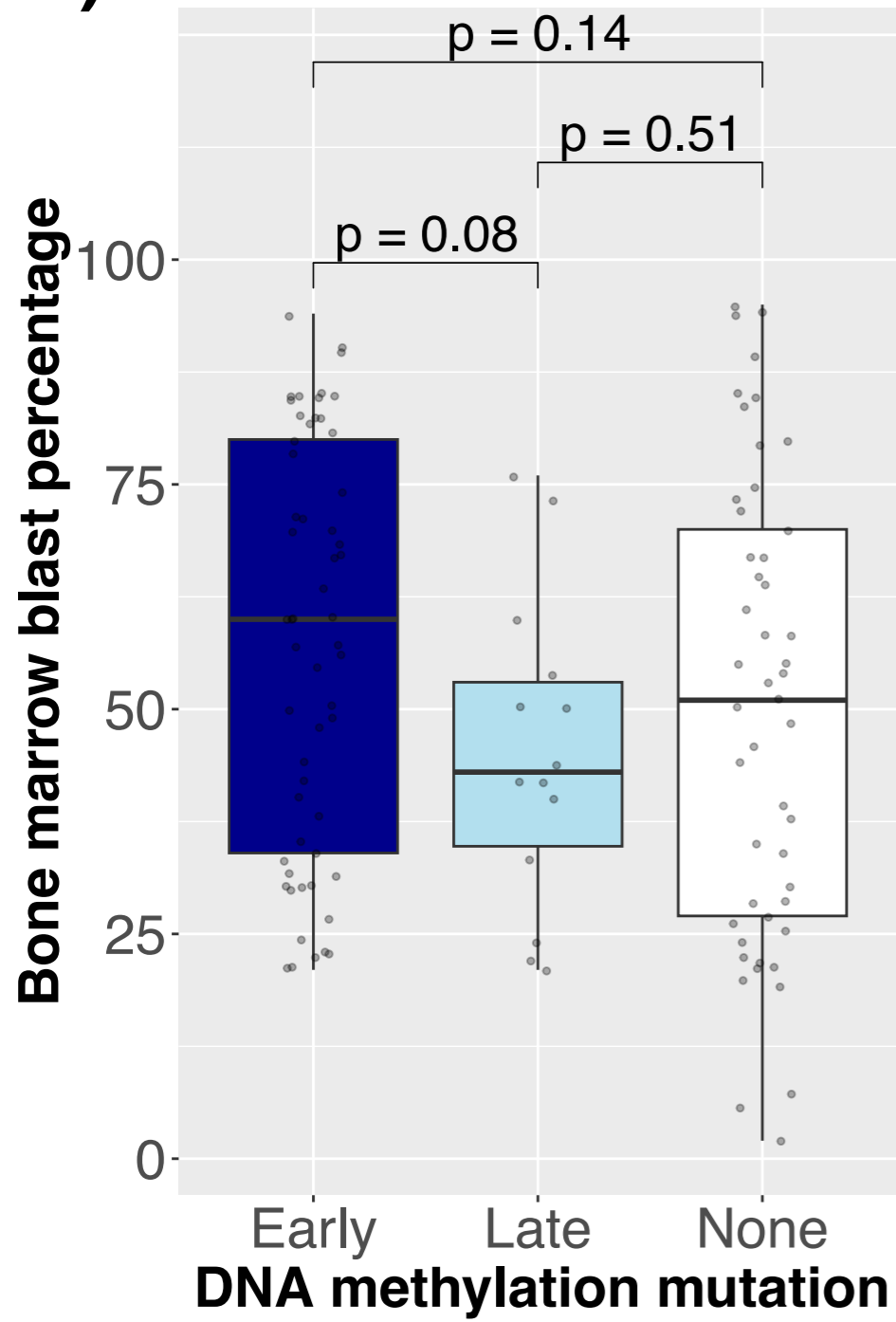
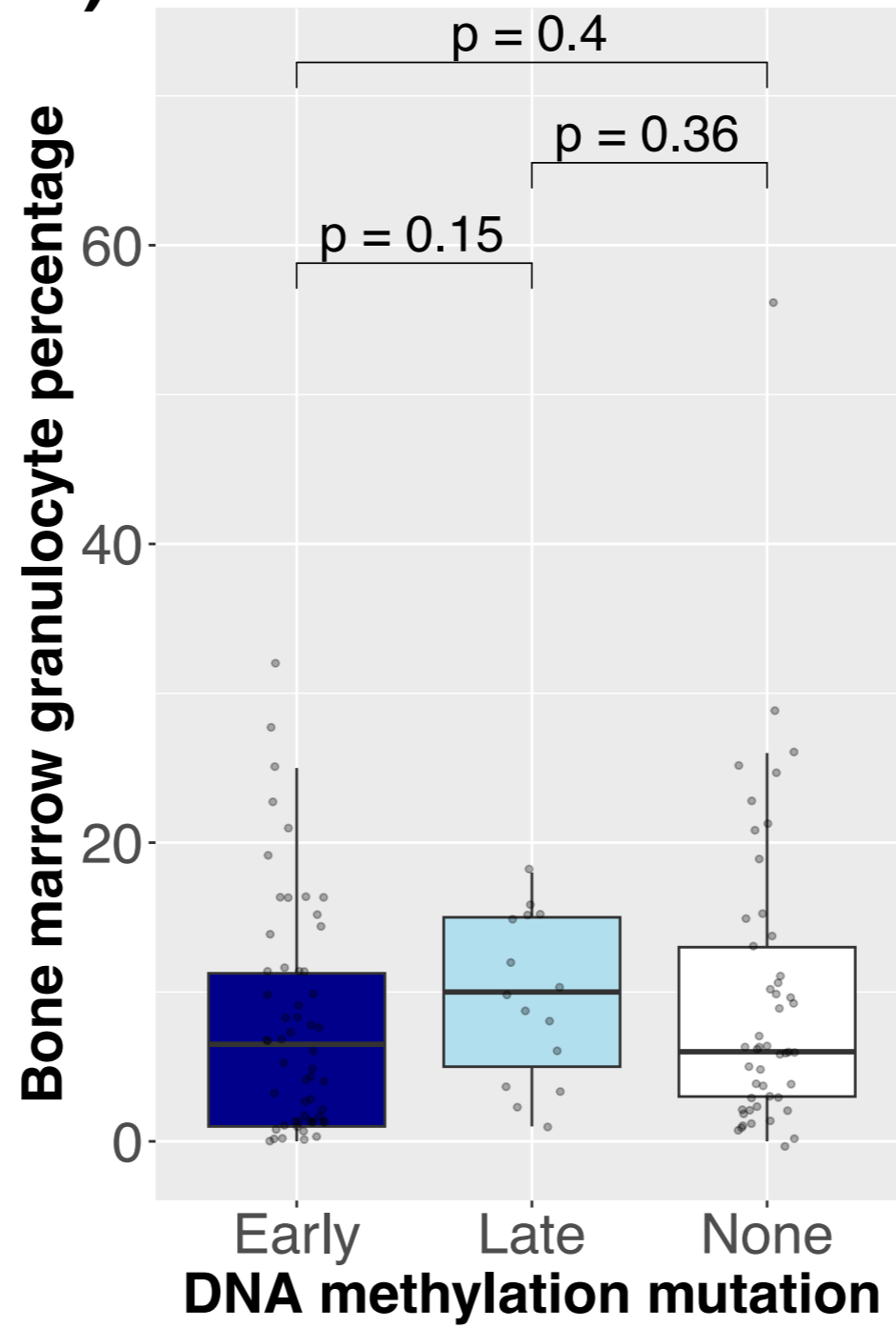


Figure 5

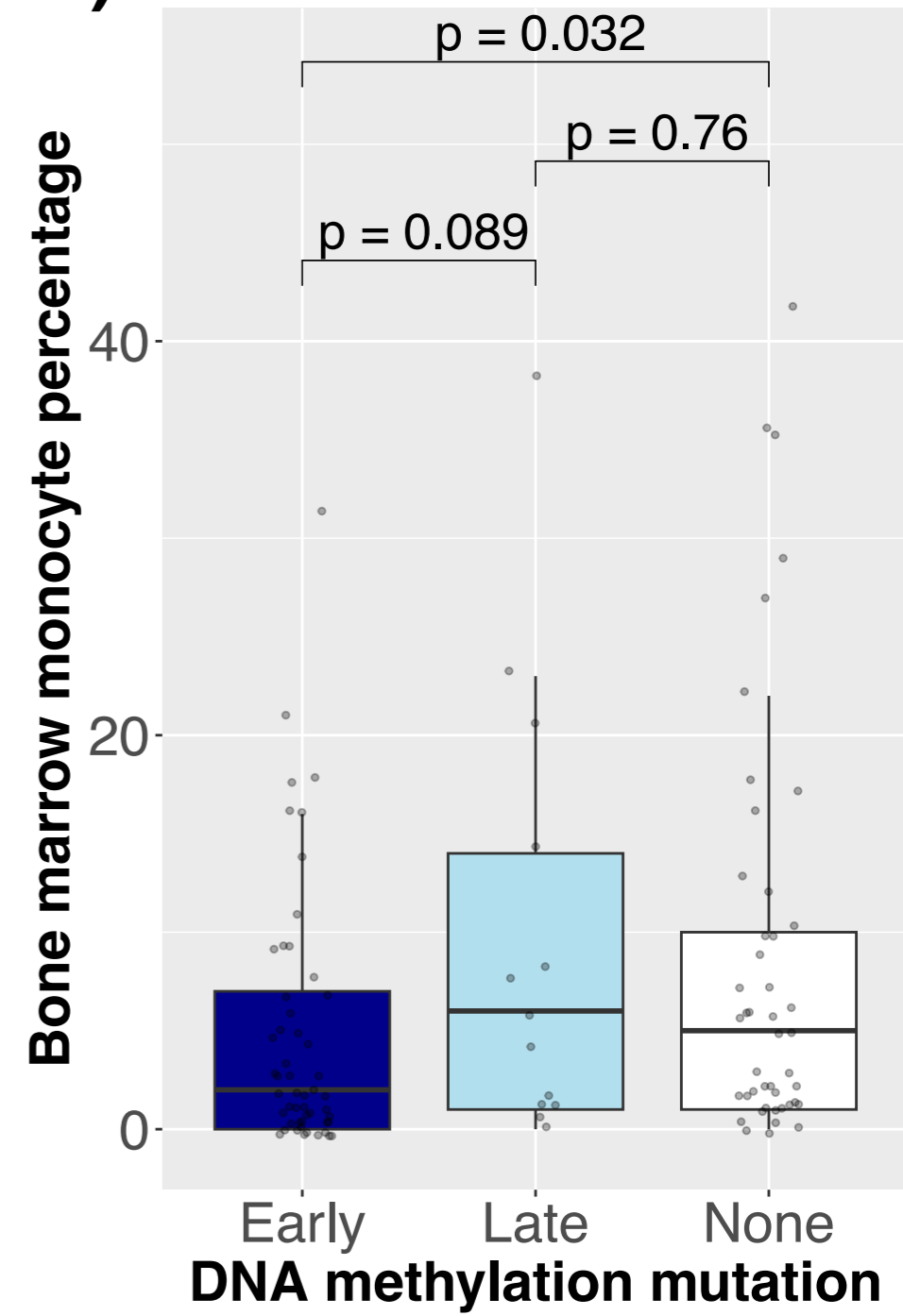
A)



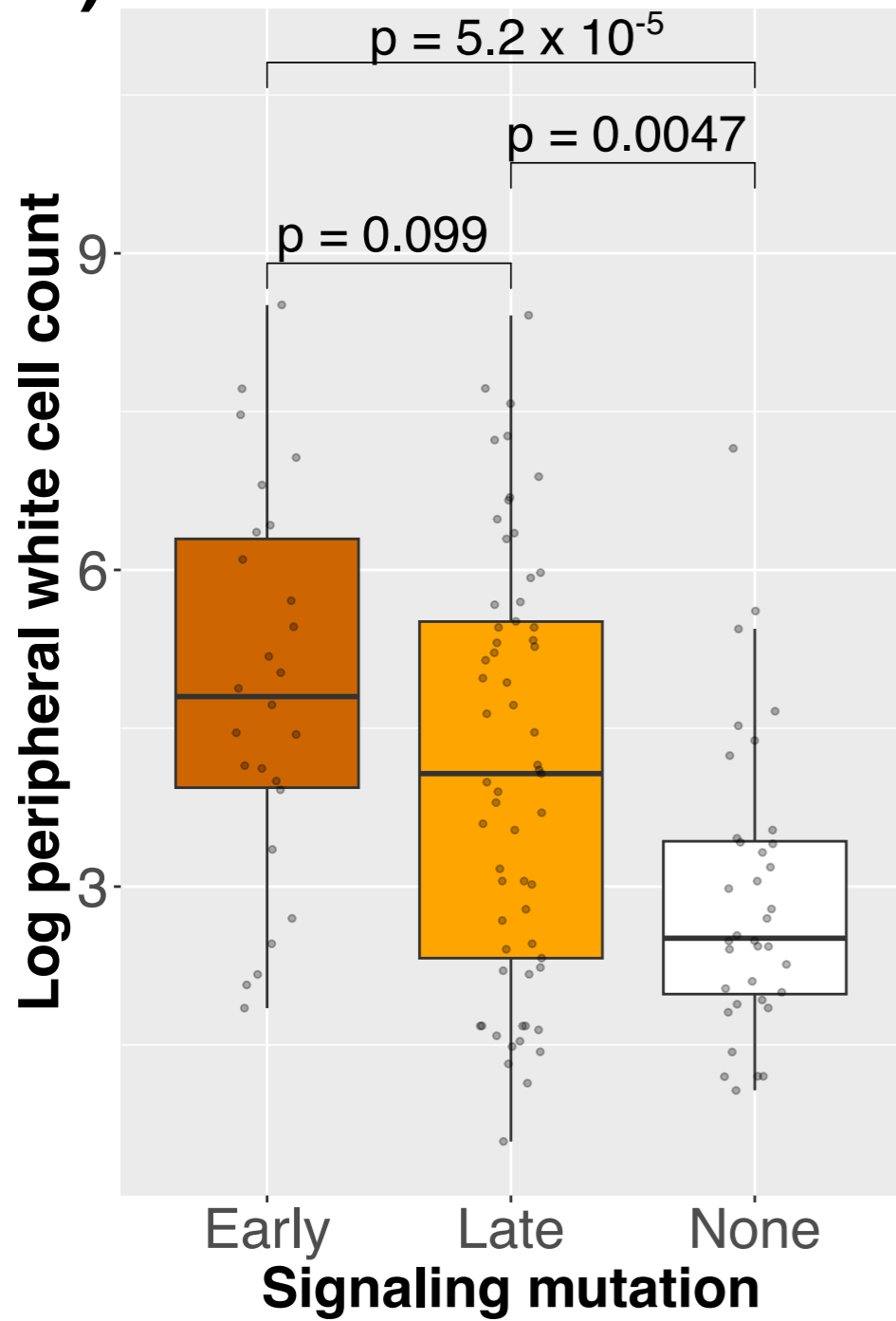
B)



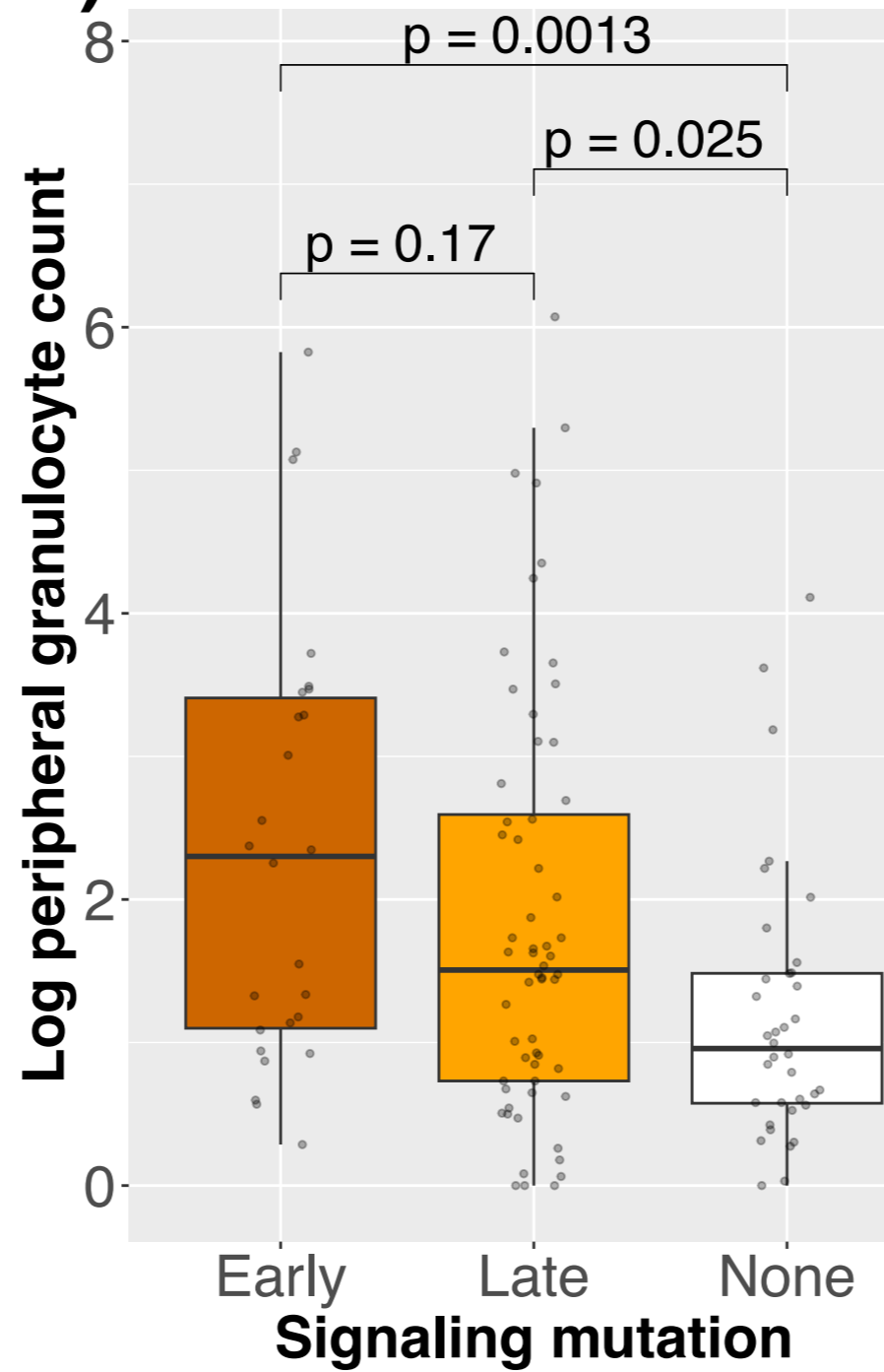
C)



D)



E)



F)

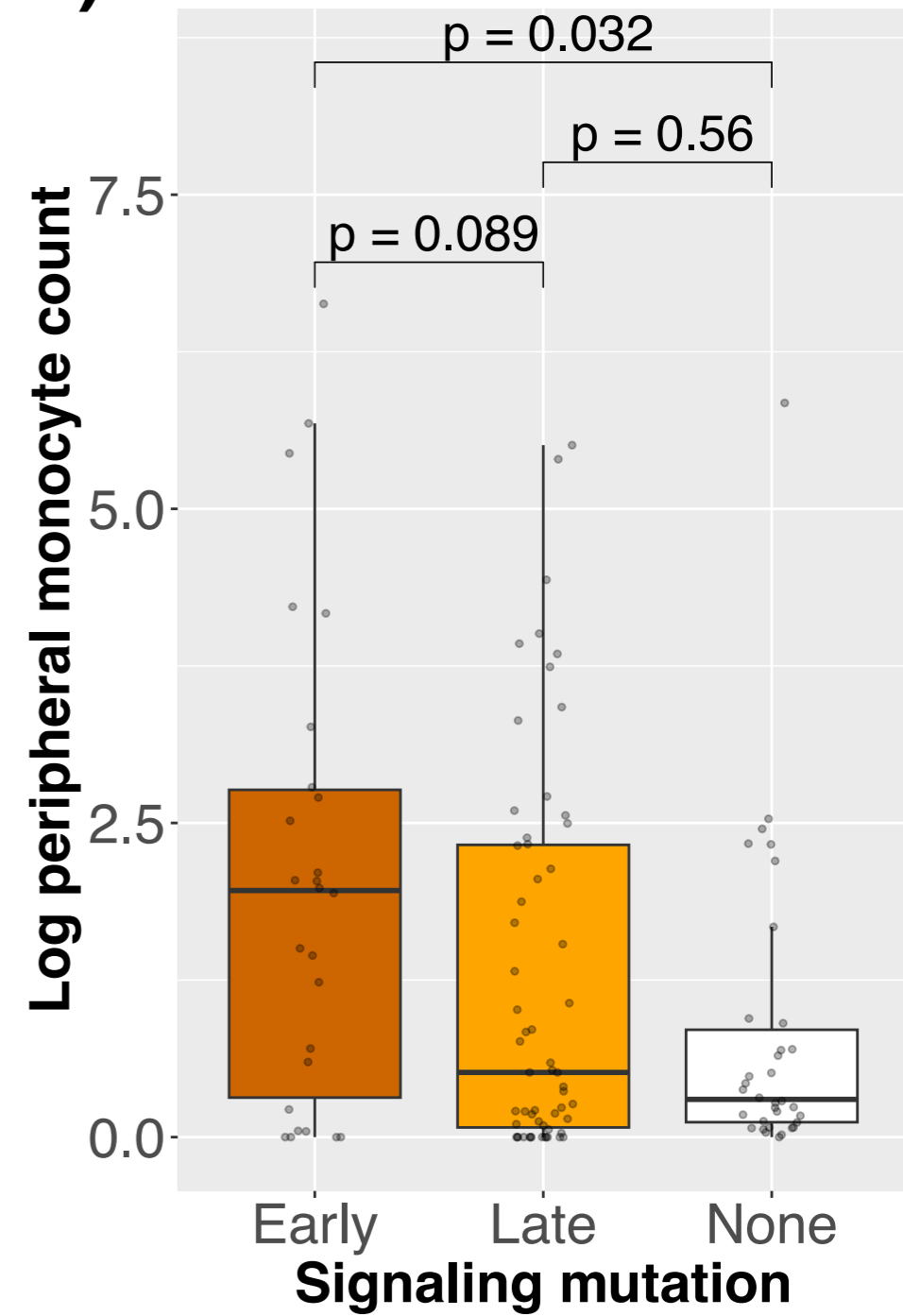
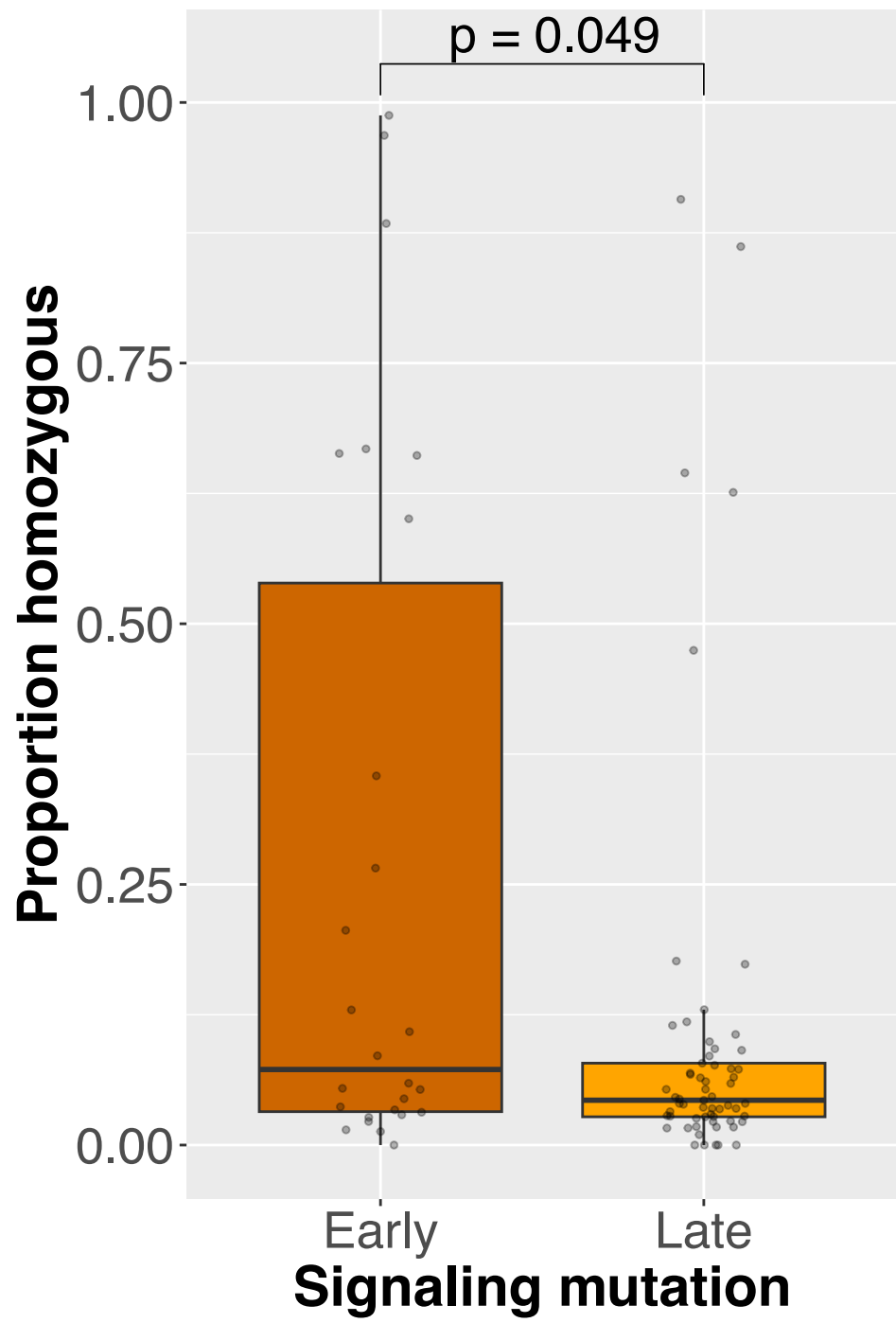
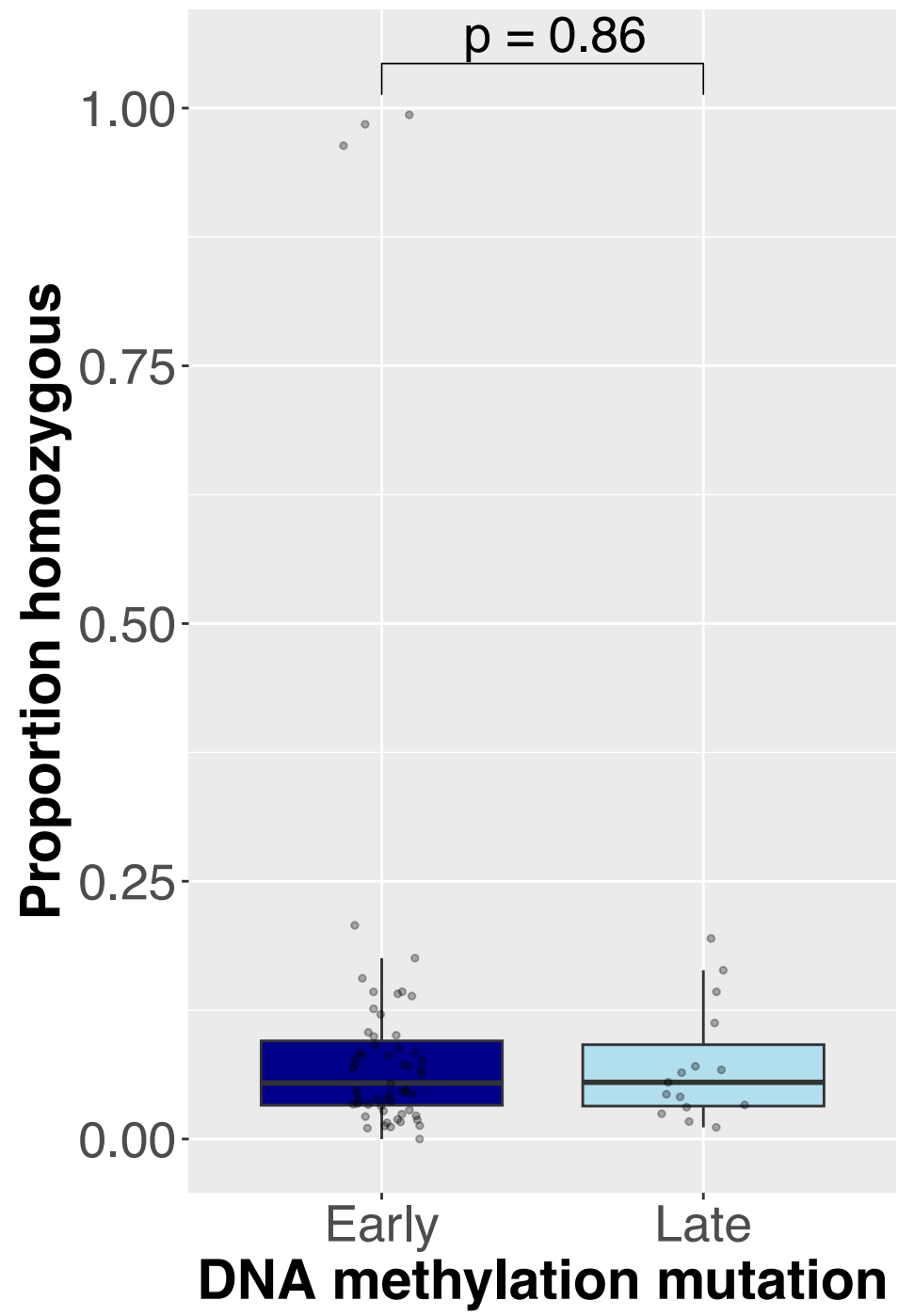


Figure 6

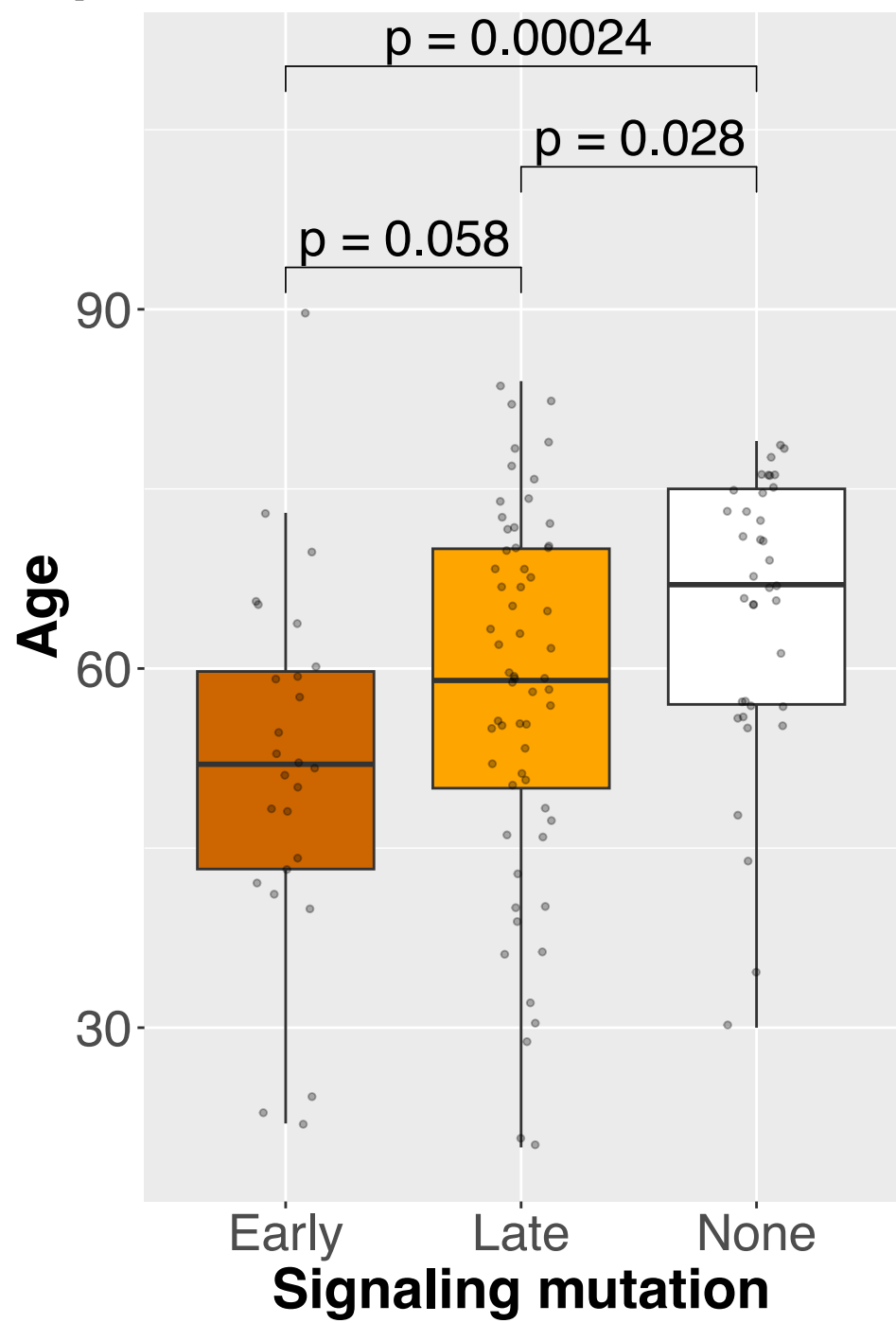
A)



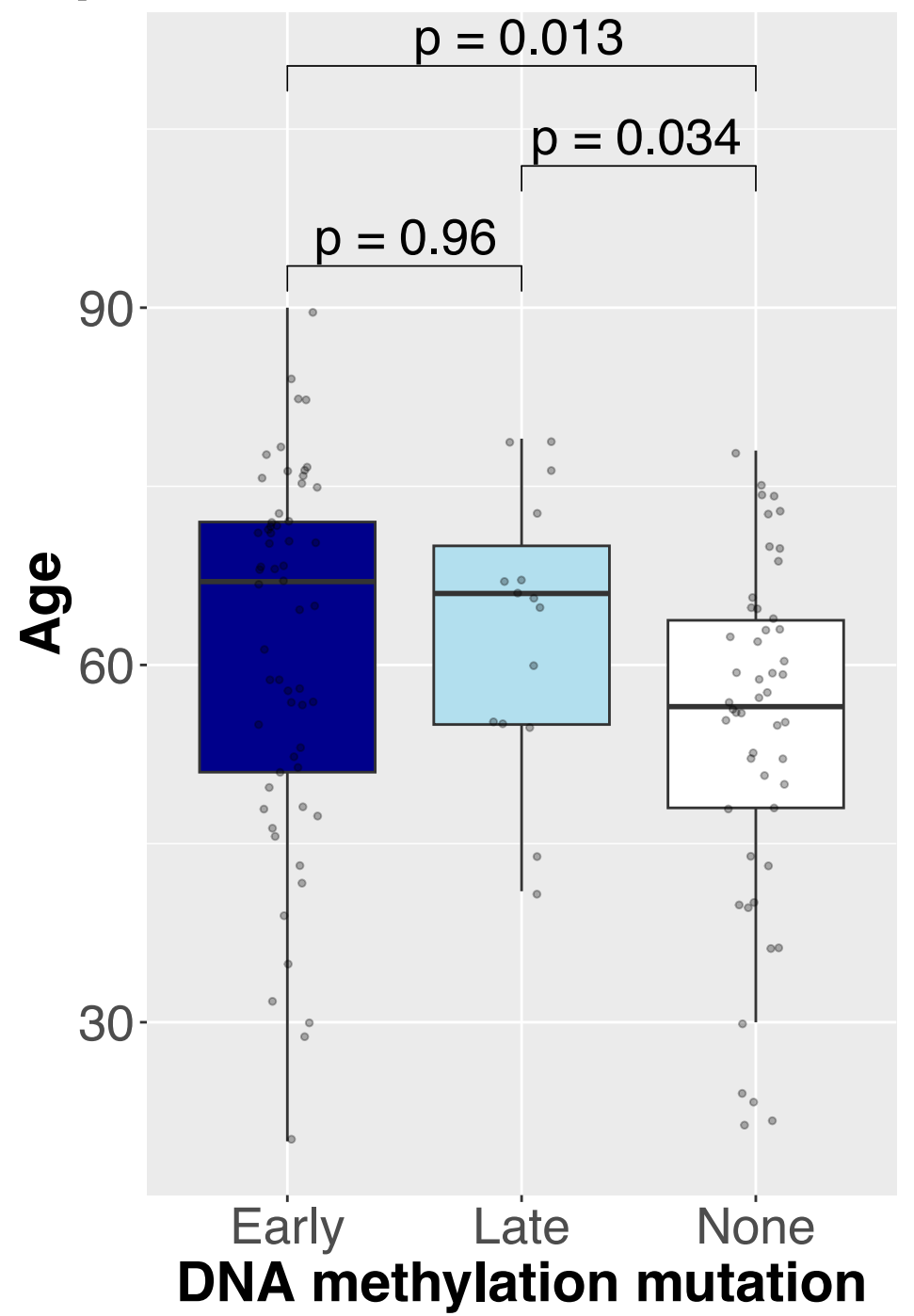
B)



C)



D)



Supplementary Files

This is a list of supplementary files associated with this preprint. Click to download.

- [Table1.xlsx](#)
- [SupplementaryTablesDocument.pdf](#)
- [SupplementalMethodsandFigures.pdf](#)